

1 **Response to Referee #1.**

2 **Old comment:** The analysis of effects of varying sun / sensor geometry has been done over 15 days (of
3 which 3 have
4 been removed) during the peak of the growing season. This misses the highest zenith angles and times
5 of different vegetation conditions. I suggest to repeat the analysis for other time periods as well to gain
6 a full picture of sun / sensor geometry effects. Furthermore, why have only NDSIs been investigated
7 and not the reflectances themselves? This information would help to understand the behaviour of the
8 NDSIs and would support the claim in the discussion that NDSIs reduce angular effects.
9

10 **Old Response:** The reason for not doing the analysis of the varying sun/sensor conditions at the point
11 in time with the highest zenith angles, is that this occurs during the dry season (two months prior
12 to the onset of the growing season) where there are no vegetation (herbaceous) influencing the
13 reflectance spectrum in the measured area. The focus of the manuscript is to investigate how
14 NDSI is coupled with vegetation parameters, and we hence choose to use the point in time with
15 most vegetation on the ground.

16 We agree that it would make a very interesting study to investigate how sun/sensor geometry
17 influences NDSI differently across the year. However, this is not a minor task and this
18 manuscript is long as is. We therefore feel that this is beyond the scope of this manuscript. But it
19 is a very good idea for a future manuscript to investigate seasonal dynamics in anisotropy of both
20 the reflectance spectrum on its own and on NDSI estimates. This is something that will hopefully
21 be possible to do in a not too distant future.

22 The reason for focusing on NDSI, and not on the anisotropy on the reflectance values
23 themselves is that it has already been done (Huber et al., 2014; Tagesson et al., 2015). The focus
24 of the paper by Tagesson et al. (2015) is to present all research activities at the Dahra field site.
25 Among them, a section of the anisotropy of the reflectance spectrum is presented. The aim of the
26 paper by Huber et al. (2014) is to present the ASD set-up and investigate the quality of the
27 measurements. A second aim is to study the effects of varying sun/sensor geometry on the
28 reflectance spectrum. Therefore, in order not to present the same information two times, the
29 effects of varying sun/sensor geometry part of this paper focus on the effects on the NDSI.
30 However, the comment is relevant and in the revised manuscript we have included a discussion
31 regarding the behaviour of the NDSI in relation to the behaviour of the reflectance spectrum and
32 referred to figures in Huber et al. (2014) and in Tagesson et al. (2015).
33

34 **New Comment:** The study uses data from 15 July 2011 until 31 December 2012. Relationships between
35 ecosystem variables and spectral indices have been investigated for the whole time period. This means
36 phenology from no living vegetation to max living vegetation is included. Therefore it is NOT APPROPRIATE to
37 restrict the analysis of effects of varying sun / sensor geometry to 15 (-3) days during the peak of the growing
38 season.

39 **New response:** In the revised version of the manuscript we have incorporated an analysis of effects of
40 varying sun/sensor geometry for four different periods over the growing season: 1) the dry season 2012 (day
41 of year (DOY) 71-85), 2) the fast growth period during the beginning of the rainy season 2011 (DOY 200-214),
42 3) the peak of the growing season in 2011 (DOY 238-253), and 4) the end of the growing season 2011 (DOY
43 278-293). However, since this analysis alone would generate 4 new figures, we have chosen in the actual
44 manuscript to present only the figures from the period with strongest effects. This is at the peak of the
45 growing season with the largest amount of photosynthesising vegetation. Remaining figures are presented in
46 a supplementary material. This analysis is referred to in the method section (L239-L242, L279-L282, L refers
47 to line number in revised manuscript), and in the results section (L313-L316).

48 **Old comment:** Why has the analysis of the relationship between reflectance / NDSI and ecosystem
49 variables been restricted to a linear relationship? E.g. other studies found a non-linear relationship between
50 reflectance and biomass due to saturation effects. Also why have only daily median reflectances / NDSIs been
51 used when GPP, LUE and FAPAR were daily integrals? Averages would be more appropriate in these cases. And
52 why have the off-nadir views not been analysed?
53

54 **Old response:** In case the linear relationship is strong, it indicates limited issues with saturation. For
55 wavelength regions where there are issues with saturations, exponential and logarithmic
56 regressions could fit better. However, in case the aim is to find wavelength regions which are as
57 sensitive as possible for investigating seasonal dynamics in an ecosystem property, wavelength
58 regions with saturation issues should be avoided. Therefore linear models are better to use than
59 non-linear models. This was the main reason for fitting linear rather than non-linear regressions.
60 There is also a practical aspect to it. Fitting the reduced major axis linear relationships using the
61 bootstrapping methodology required a full month of processing for these 4 variables (GPP, LUE, FAPAR, and
62 biomass). In case we would try several other regression models, these would require
63 several months of processing.

64 Median values were used in order to minimise the influence of errors in the analysis. Median
65 provides the most common model output and it is thereby more robust against outliers than
66 average values. This info was provided in the manuscript, but it was not mentioned the first time
67 that median values were used. Thank you for pointing this out to us; it has been corrected in the
68 revised manuscript.

69 We have investigated the seasonal dynamics in the off-nadir views as well, but as seen in the
70 figure below, there was no difference in seasonal dynamics for the different viewing angles. We
71 thereby choose to only use the nadir one, as it would not make any difference in the analysis.

72 **New comment:** This is not a satisfactory response. Many studies have found non-linear relationships to
73 work much better than linear ones. Therefore, restricting the analysis to linear relationships might not yield the
74 best wavelength combinations.

75 **New response:** In the revised manuscript, we have fitted exponential regression models between the
76 ecosystem properties and the NDSI combinations. However, we cannot do this using a bootstrapping
77 methodology as we do not have the computer capacity for doing these types of fitting 200 times for all
78 wavelength combination (1451*1451 wavelength combinations).

79 There were few wavelength combinations which had stronger relationships using an exponential
80 regression rather than a linear, and the exponential models did not significantly improve the relationships.
81 We hence choose to present these results only in a supplementary material, and in the main text we refer to
82 the supplementary material (L261-L264).

83 **Old comment:** page 3330, lines 11-14: This is not the reason for the saturation of the NDVI. The NDVI
84 saturates at high biomass because the NIR reflectance is much larger than the red reflectance. NDVI therefore
85 reduces to R_{NIR} / R_{NIR} which equals 1.
86

87 **Old response:** We agree with you, and we are talking about the same thing, we are just using
88 different phrasing, where you consider it from an equation point of view, we consider it from a
89 leaf optical property point of view.

90 All vegetation indices using red will suffer from saturation problems. The reason for this is
91 related to the fact that there are only so many photons striking a plant leaf and at a certain point, the
92 chlorophyll absorbs nearly all the red energy to the point where no matter how much
93 vegetation you add, more photons cannot be absorbed because they are already all absorbed. It is
94 normally the red band that saturates. So any index using the red energy will suffer from the same
95 limitation. For example, the Enhanced Vegetation Index (EVI) is not supposed to saturate as
96 badly because in the equation empirical constants have been added to put more weight in the
97 NIR spectrum that preserves sensitivity to higher loads of biomass (more layers of leafs) because
98 here much more radiation is transmitted and reflected from the leaves.
99

100 **New Comment:** No, we are not talking about the same thing!!! I say the saturation stems from the specific
101 equation applied (i.e. normalised difference). You say the saturation stems from the red band showing no
102 changes. $R_{NIR} \ll R_{RED}$ leads to $NDVI = R_{NIR} / R_{NIR} = 1$. If you use a different index, e.g. the simple ratio
103 R_{RED} / R_{NIR} there are not saturation issues if R_{RED} is small and changes little as long as R_{NIR} still changes.

104 **New response:** We are sorry that we misinterpreted your comment. However, the explanation given in
105 the discussion is still valid (L435-L441).

106 Also, we are sorry but this explanation is incorrect. The smallest ratio between two different HCRF
107 measurements from the same day that we have in our data set is 0.01, i.e. the same thing as if red was 1% of
108 NIR. Assume that red is 1% of NIR; it generates a SR of 0.01, whereas it generates an NDVI of 0.98. Assume
109 that the ratio red/NIR rises to 0.015, i.e. a SR of 0.015. This would yield an NDVI of 0.97. This means that a
110 0.005 increase in red generates a 0.005 change in SR, but a 0.01 change in NDVI. NDVI is thereby more

111 sensitive than SR to changes in reflectance values << than reflectance in the reference band. The saturation
112 effect seen in NDVI can hence not be explained from this equation point of view.

113 We can easily find a handful of references supporting our explanation of NDVI given in the earlier
114 response. But, since this entire discussion arose from the phrasing of a single sentence in the discussion, a
115 sentence which has been changed, we hope that we can leave this minor detail behind.

116

117 **Response to Referee #2.**

118 The authors have made substantial changes to the manuscript so it has improved its clarity. However, I think
119 there are still several minor changes that must be considered. My specific edits/comments are below (lines
120 refer to manuscript version 3).

121
122 **Response: Thank you very much for helpful comments that has helped improving the manuscript a great**
123 **deal.**

124
125 Line 31. Remove “also”

126
127 Line 33. Add “:” after ...properties were....

128
129 Line 34 Remove “,” After GPP

130
131 Line 35 Specify which blue wavelengths

132
133 **Response: These things have been taken care of in the revised manuscript.**

134
135 Lines 36-37 Review the use of commas

136
137 **Response: We have asked two native English speakers about this sentence. Both state that it is**
138 **grammatically correct. We thereby do not know how to review the use of commas.**

139
140 Lines 45-46 Avoid repetition (properties)

141
142 Lines 49-50 “For example” between commas

143
144 Line 67 “at the present state” between commas

145
146 **Response: These things have been taken care of in the revised manuscript.**

147
148 Lines 100-102. These effects have been also explored from multiangular data sets acquired from tower based
149 sensor such as the AMSPEC (see Hilker, T., Coops, N.C., Hall, F.G., Black, T.A., Wulder, M.A., Nestic, Z., &
150 Krishnan, P. (2008). Separating physiologically and directionally induced changes in PRI using BRDF models.
151 Remote Sensing of Environment, 112, 2777-2788)

152
153 **Response: Thank you very much. This reference has been included in the introduction (L102, L means Line in**
154 **revised manuscript)**

155
156 Lines 127-128. Avoid repetition (dominate)

157
158 Lines 146-147 In order to avoid repetition (and) I suggest to divide this sentence in two:USA). Data
159 were sampled every 30 s and stored.....

160

161 Line 183 Spelling error (dominant)

162
163 **Response: These things have been taken care of in the revised manuscript.**

164
165 Line 237 Filtered means removed? If not please, specify how the data was filtered

166
167 **Response: Yes, filter means removed. This has been clarified in the revised manuscript (L284-288).**

168
169 Line 247 UTC times? Please specify here and throughout the text when time references are included

170
171 **Response: Yes UTC times. This has been specified throughout the revised text.**

172
173 I have an additional question regarding this analysis on the effect of solar zenith angles in the NDSI. Taking into
174 account that the range of measurements includes acquisitions from early in the morning to late afternoon, is it
175 possible that the differences in the COV are not only due to the sensitivity of the indices to the solar angles but
176 also to their sensitivity to the diurnal changes on vegetation status (i.e. water content)?

177
178 **Response: Thank you for pointing this out to us. Yes, naturally there can also be diurnal variability in the**
179 **vegetation affecting the diurnal variability in the reflectance spectrum. This has been included as a point of**
180 **discussion in the revised manuscript (L395-L402):**

181
182 **“A strong diurnal dynamic does not necessarily mean a poor NDSI. For example, the photochemical**
183 **reflectance index (PRI) was created for assessing diurnal dynamics in the xanthophyll cycle activity (Gamon**
184 **et al., 1992). Stomatal closure due to high temperatures could also influence diurnal dynamics of vegetation**
185 **properties (Lasslop et al., 2010), and hence the diurnal dynamics of NDSI. However, diurnal variation in**
186 **reflectance caused by diurnal variability in vegetation status is assumed minor in relation to the diurnal**
187 **variability caused by changes in solar zenith angles. Additionally, in our study we are interested in**
188 **relationships in seasonal dynamics between ecosystem properties and NDSI; diurnal variation can thereby**
189 **interfere and introduce uncertainty in such relationships.”**

190 Lines 275-276 Avoid repetition (thereby)

191
192 **Response: This has been taken care of in the revised manuscript.**

193
194 Line 281 The ANIF threshold (s)?

195
196 **Response: Yes, thresholds. This has been taken care of in the revised manuscript (L282)**

197
198 Lines 294-295. Avoid repetition (hyperspectral HCRF). I suggest:to clearly illustrate these seasonal
199 dynamics, the ratio.....

200
201 **Response: We have changed the sentence according your suggestion.**

202
203 Line 311 But were these water absorption bands not previously removed?

204

205 **Response: Thank you for pointing this out. In the revised manuscript we have changed the figures so that,**
206 **the upper right corner shows unfiltered data and the lower left corner shows filtered data. This sentence has**
207 **also been removed.**
208

209 Line 328 This correlation is opposite to expected (if related with water absorption) so I am not sure if the
210 reference to Thenkabail et al 2012 is appropriate here.

211
212 **Response: Thank you for pointing this out. This sentence has been removed and these things are instead**
213 **discussed in the discussion (L422-L432).**
214

215 Lines 378-379 simplify the sentence. I suggest:with large differences in effects of variable solar zenith
216 angles (Fig. 6 in Huber et al. 2014) and variable view zenith angles.....

217
218 Line 380in the case (of)?...

219
220 **Response: These things have been taken care of in the revised manuscript.**
221

222 Lines 373-784. I think it would be necessary to discuss here the results found in comparison with other authors
223 that have analyzed this sun-sensor geometry using spectral indices. For example by comparing with the results
224 found by Huber et al 2014 (section 3.4) with NDVI and SWISI. Have other authors reported larger effects in low
225 index values? And in NIR/SWIR indices compared with VIS/NIR?

226
227 **Response: We have included a comparison of these results to other studies in the revised manuscript (L386-**
228 **394):**
229

230 **“The relative HCRF difference between NIR and SWIR is lower as compared to indices including the VIS**
231 **domain; NIR/SWIR based indices thereby generate lower NDSI values with higher sensitivity to sun-sensor**
232 **geometry generated differences between included wavelengths (Fig. 3 and 4). This can also be seen in the**
233 **SIWSI/NDVI comparison by Huber et al (2014); SIWSI had large relative differences depending on viewing**
234 **angle (~70%), whereas NDVI had relatively small (~5%) (Fig. 10 in Huber et al. (2014)). Fensholt et al. (2010)**
235 **showed the same to be true in a comparison between SIWSI and NDVI based on MODIS data: SIWSI was**
236 **insensitive to day-to-day variations in canopy water status due to effects of solar zenith angles and sensor**
237 **viewing geometry blurring the signal.”**
238

239 Lines 406-411. This results are not only interesting but surprising so I think more elaboration on a possible
240 explanation is needed

241
242 **Response: We have revised the discussion to (L422-L432):**
243

244 **“Previous studies have generally shown positive relationships between NIR HCRF and biomass since a large**
245 **fraction of NIR radiation is reflected in green healthy vegetation to avoid overheating (e.g. Hansen and**
246 **Schjoerring, 2003; Asner, 1998). Here, a strong negative relationship between NIR HCRF and dry weight**
247 **biomass is generally observed (Fig. 5a), indicating stronger NIR absorption with increased biomass. However,**
248 **a strong positive NIR HCRF correlation with vegetation water content was seen (figure not shown). A**
249 **possible explanation could be that the sampled biomass at the end of the rainy season contained some**
250 **senescent vegetation, and a correlation against vegetation water content is hence closer to green healthy**

251 **vegetation. This relationship is however interesting and should be studied further to better understand the**
252 **respective importance of canopy water and leaf internal cellular structure for the NIR HCRF of herbaceous**
253 **vegetation characterised by erectophile leaf angle distribution in semi-arid regions.”**
254

255 Line 740 (table 1) I suggest replace “information about the sensor set-up” by “information about the
256 instrumental set-up”. I would also suggest to add a column with information on the time period of each
257 dataset .

258
259 **Response: We have changed to instrumental set-up in the revised table 2. We have also included a column**
260 **with first year of measurements, and that if the reader wants more information regarding the sensor set up,**
261 **we refer to (Tagesson et al., 2015). In the supplementary material of (Tagesson et al., 2015), all information**
262 **about the time periods of the different measured variables are included.**
263

264 Line 747 to 751 (table 2). I would suggest adding the Relative Root Mean Square Error (RRMSE) as it facilitates
265 the comparison between variables with different ranges.(see Richter, K., Atzberger, C., Hank, T. B., and
266 Mauser, W.: Derivation of biophysical variables 16 from Earth observation data: validation and statistical
267 measures, APPRES, 6, 063557-063551-17 063557-063523, 10.1117/1.jrs.6.063557, 2012.)

268
269 **Response: In the previous version of the manuscript, we had included RRMSE in the text. In the revised**
270 **version, we have also included a column with RRMSE in Table 2.**
271

272 Figure 2 In figure 2a the a) overlaps the info, maybe can be moved

273
274 **Response: The axis of Fig 2a has been changed in order to make sure that the a) is not overlapping the data.**

275 Figures 3, 4 and 6. If the spectral bands between 350-390 and 1300-1500 have been removed shouldn't be
276 included in these graphs. Again it is not clear to me if this information was removed (as in figure 5) or filtered.

277 **Response: These data were removed, and this has been clarified in the revised manuscript (L279-299). We**
278 **have revised Fig. 3 and fig 4, so that the upper right corner shows all data, and the lower left corner shows**
279 **filtered data.**

280 **References:**

281 Asner, G. P.: Biophysical and Biochemical Sources of Variability in Canopy Reflectance, Remote Sens.
282 Environ., 64, 234-253, [http://dx.doi.org/10.1016/S0034-4257\(98\)00014-5](http://dx.doi.org/10.1016/S0034-4257(98)00014-5), 1998.

283 Fensholt, R., Huber, S., Proud, S. R., and Mbow, C.: Detecting Canopy Water Status Using Shortwave
284 Infrared Reflectance Data From Polar Orbiting and Geostationary Platforms, IEEE J. Sel. Top. Appl., 3,
285 271-285, 10.1109/jstars.2010.2048744, 2010.

286 Gamon, J. A., Peñuelas, J., and Field, C. B.: A narrow-waveband spectral index that tracks diurnal
287 changes in photosynthetic efficiency, Remote Sens. Environ., 41, 35-44,
288 [http://dx.doi.org/10.1016/0034-4257\(92\)90059-S](http://dx.doi.org/10.1016/0034-4257(92)90059-S), 1992.

289 Hansen, P. M., and Schjoerring, J. K.: Reflectance measurement of canopy biomass and nitrogen
290 status in wheat crops using normalized difference vegetation indices and partial least squares

291 regression, *Remote Sens. Environ.*, 86, 542-553, [http://dx.doi.org/10.1016/S0034-4257\(03\)00131-7](http://dx.doi.org/10.1016/S0034-4257(03)00131-7),
292 2003.

293 Huber, S., Tagesson, T., and Fensholt, R.: An automated field spectrometer system for studying VIS,
294 NIR and SWIR anisotropy for semi-arid savanna, *Remote Sens. Environ.*, 152, 547–556, 2014.

295 Lasslop, G., Reichstein, M., and Papale, D.: Separation of net ecosystem exchange into assimilation
296 and respiration using a light response curve approach: critical issues and global evaluation, *Global*
297 *Change Biol.*, 16, 187-209, 2010.

298 Tagesson, T., Fensholt, R., Guiro, I., Rasmussen, M. O., Huber, S., Mbow, C., Garcia, M., Horion, S.,
299 Sandholt, I., Rasmussen, B. H., Göttsche, F. M., Ridler, M.-E., Olén, N., Olsen, J. L., Ehammer, A.,
300 Madsen, M., Olesen, F. S., and Ardö, J.: Ecosystem properties of semi-arid savanna grassland in West
301 Africa and its relationship to environmental variability, *Global Change Biol.*, 21, 250-264, doi:
302 10.1111/gcb.12734, 2015.

303

304

305 **Relevant changes made in the manuscript**

306

307 • A supplementary material has been included with an analysis of seasonal dynamics in effects of solar and
308 sensor viewing geometry and an analysis of differences between exponential and linear regression
309 models.

310 • In the filtering of data, we have taken into account the effect of sensor and viewing geometry for
311 different parts of the growing season.

312 • It has been clarified that the water absorption band was removed within the filtering procedure.

313 • In the discussion we have added discussions of results of other studies in the effects of sensor and
314 viewing geometry, a discussion of effects of diurnal variability in vegetation status, and extended the
315 discussion regarding the biomass correlation to HCRF.

316

317

318 **Deriving seasonal dynamics in ecosystem properties of semi-**
319 **arid savanna grasslands from in situ based hyperspectral**
320 **reflectance**

321
322 **Torbern Tagesson^{*,1}, Rasmus Fensholt¹, Silvia Huber², Stephanie Horion¹, Idrissa Guiro³, Andrea Ehammer¹,**
323 **Jonas Ardo⁴**

324

325 ¹Department of Geosciences and Natural Resource Management, University of Copenhagen, Øster Voldgade
326 10, DK-1350 Copenhagen, Denmark; E-Mails: torbern.tagesson@ign.ku.dk, rf@ign.ku.dk,
327 stephanie.horion@ign.ku.dk, andrea.ehammer@ign.ku.dk

328

329 ²DHI GRAS A/S, Agern Allé 5, DK-2970 Hørsholm, Denmark; E-mail: shu@dhi-gras.com

330

331 ³Laboratoire d'Enseignement et de Recherche en Géomatique, Ecole Supérieure Polytechnique, Université
332 Cheikh Anta Diop de Dakar, BP 25275 Dakar-Fann, Senegal; E-mail: idyguiro@yahoo.fr

333

334 ⁴Department of Physical Geography and Ecosystem Science, Lund University, Sölvegatan 12, SE-223 62 Lund,
335 Sweden, E-mail: jonas.arde@nateko.lu.se

336

337 *Correspondence to: Torbern Tagesson; torbern.tagesson@ign.ku.dk, Tel. nr: +46-704 99 39 36, Fax nr: +45 35
338 32 25 01, Department of Geosciences and Natural Resource Management, University of Copenhagen, Øster
339 Voldgade 10, DK-1350 Copenhagen, Denmark

340 **Abstract**

341 This paper investigates how hyperspectral reflectance (between 350 and 1800 nm) can be used to infer
342 ecosystem properties for a semi-arid savanna grassland in West Africa using a unique in situ based multi-
343 angular dataset of hemispherical conical reflectance factor (HCRF) measurements. Relationships between
344 seasonal dynamics in hyperspectral HCRF, and ecosystem properties (biomass, gross primary productivity
345 (GPP), light use efficiency (LUE), and fraction of photosynthetically active radiation absorbed by vegetation
346 (FAPAR)) were analysed. HCRF data (ρ) were used to study the relationship between normalised difference
347 spectral indices (NDSI) and the measured ecosystem properties. Finally, ~~also~~ the effects of variable sun sensor
348 viewing geometry on different NDSI wavelength combinations were analysed. The wavelengths with the
349 strongest correlation to seasonal dynamics in ecosystem properties were: shortwave infrared (biomass), the
350 peak absorption band for chlorophyll a and b (at 682 nm) (GPP), the oxygen A-band at 761 nm used for
351 estimating chlorophyll fluorescence (GPP, and LUE), and blue wavelengths (ρ_{412}) (FAPAR). The NDSI with the
352 strongest correlation to: i) biomass combined red edge HCRF (ρ_{705}) with green HCRF (ρ_{587}), ii) GPP combined
353 wavelengths at the peak of green reflection (ρ_{518}, ρ_{556}), iii) ~~the~~ LUE combined red (ρ_{688}) with blue HCRF (ρ_{436}),
354 and iv) FAPAR combined blue (ρ_{399}) and near infrared (ρ_{1295}) wavelengths. NDSI combining near infrared and
355 shortwave infrared were strongly affected by solar zenith angles and sensor viewing geometry, as were many
356 combinations of visible wavelengths. This study provides analyses based upon novel multi-angular
357 hyperspectral data for validation of earth observation based properties of semi-arid ecosystems, as well as
358 insights for designing spectral characteristics of future sensors for ecosystem monitoring.

359 **1. Introduction**

360 Hyperspectral measurements of the Earth's surface provide relevant information for many ecological
361 applications. An important tool for spatial extrapolation of ecosystem functions ~~and properties~~ is to study how
362 spectral properties are related to in situ measured ecosystem properties. These relationships found the basis
363 for up-scaling using earth observation (EO) data. Continuous in situ measurements of hyperspectral reflectance
364 in combination with ecosystem properties are thereby essential for improving our understanding of the
365 functioning of the observed ecosystems. Strong relationships have, for example, been found between
366 information in the reflectance spectrum and ecosystem properties such as leaf area index (LAI), fraction of
367 photosynthetically active radiation (PAR) absorbed by the vegetation (FAPAR), light use efficiency (LUE),
368 biomass, vegetation primary productivity, vegetation water content, and nitrogen and chlorophyll content (e.g.
369 Thenkabail et al., 2012; Tagesson et al., 2009; Gower et al., 1999; Sjöström et al., 2009; Sims and Gamon,
370 2003). In situ observations of spectral reflectance are also important for parameterisation and validation of
371 canopy reflectance models, and space and airborne products (Coburn and Peddle, 2006).

372 Very few sites across the world exist with an instrumental setup designed for multi-angular continuous
373 hyperspectral measurements. Leuning et al. (2006) present a system mounted in a 70 m tower above an
374 evergreen Eucalyptus forest in New South Wales Australia, which measures spectral hemispherical conical
375 reflectance factors (HCRF)¹ hourly throughout the year between 300 and 1150 nm at four azimuth angles.
376 Hilker et al. (2007) and Hilker et al. (2010) describe an automated multi-angular spectro-radiometer for
377 estimation of canopy HCRF (AMSPEC) mounted on a tower above a coniferous forest in Canada. Spectral HCRF
378 is sampled between 350 and 1200 nm year round under different viewing and sun angle conditions, achieved

¹ Different reflectance terminologies have been used to inform on spectral measurements in the field by the remote sensing community leading to suggestions to the proper use of the terminology (Martonchik et al., 2000). All field spectro-radiometers measure HCRF (hemispherical conical reflectance) if the field of view (FOV) of the sensor is larger than 3° (Milton et al., 2009) and is therefore used throughout this paper to support the correct inference and usage of reflectance products (Schaepman-Strub et al., 2006; Milton et al., 2009).

379 by collection of data in a near 360° view around the tower with adjustable viewing zenith angles. Even though
380 in situ measurements of multi-angular hyperspectral HCRF are fundamental for the EO research community,
381 such datasets are still rare and, at the present state, they do not cover different biomes at the global scale
382 (Huber et al., 2014).

383 There are many methods for analysing relationships between hyperspectral reflectance and ecosystem
384 properties, such as multivariate methods, derivative techniques, and radiative transfer modelling (Bowyer and
385 Danson, 2004; Ceccato et al., 2002; Danson et al., 1992; Roberto et al., 2012). Still, due to its simplicity, the
386 combination of reflectance into vegetation indices is the major method for up-scaling using EO data. By far, the
387 most commonly applied vegetation indices are those based on band ratios, e.g. the normalised difference
388 vegetation index (NDVI), which is calculated by dividing the difference in the near infrared (NIR) and red
389 wavelength bands by the sum of the NIR and red bands (Tucker, 1979; Rouse et al., 1974). The NIR radiance is
390 strongly scattered by the air-water interfaces between the cells whereas red radiance is absorbed by
391 chlorophyll and its accessory pigments (Gates et al., 1965). The normalization with the sum in the denominator
392 is a mean to reduce the effects of solar zenith angle, sensor viewing geometry, and atmospheric errors as well
393 as enhancing the signal of the observed target (e.g. Qi et al., 1994; Inoue et al., 2008).

394 Wavelength specific spectral reflectance is known to be related to leaf characteristics such as chlorophyll
395 concentration, dry matter content, internal structure parameters and equivalent water thickness (Ceccato et
396 al., 2002). Hyperspectral reflectance data can be combined into a matrix of normalised difference spectral
397 indices (NDSI), following the NDVI rationing approach. Correlating the NDSI with ecosystem properties provides
398 a way for an improved empirically based understanding of the relationship between information in the
399 reflectance spectrum with ground surface properties (e.g. Inoue et al., 2008). Several studies have analysed
400 relationships between hyperspectral HCRF, NDSI, and ecosystem properties (e.g. Thenkabail et al., 2000; Cho et

401 al., 2007; Psomas et al., 2011; Inoue et al., 2008; Gamon et al., 1992; Feret et al., 2008; Thenkabail et al., 2012).
402 Still, it is extremely important to examine these relationships for different ecosystems across the earth and
403 investigate their applicability for different environmental conditions and under different effects of biotic and
404 abiotic stresses.

405 A strong correlation between an NDSI and an ecosystem property does not necessarily indicate that the NDSI
406 is a good indicator of vegetation conditions to be applied to EO systems. Visible, NIR and shortwave infrared
407 (SWIR) have different sensitivity to variations in solar zenith angles, stand structure, health status of the
408 vegetation, vegetation and soil water content, direct/diffuse radiation ratio, and sensor viewing geometry. The
409 influence of sun-sensor geometry on the reflected signal has been studied using radiative transfer models and
410 airborne (e.g. AirMISR) as well as satellite-based data from instruments such as CHRIS-PROBA, MISR or POLDER
411 (Huber et al., 2010; Maignan et al., 2004; Javier García-Haro et al., 2006; Jacquemoud et al., 2009; Verhoef and
412 Bach, 2007; Laurent et al., 2011). However, effects of variable sun angles and sensor viewing geometries are
413 not well documented in situ for different plant functional types of natural ecosystems except for some
414 individual controlled experiments ~~based on the use of field goniometers~~ (Hilker et al., 2008; Sandmeier et al.,
415 1998; Schopfer et al., 2008). Improved knowledge regarding the influence from sun-sensor variability on
416 different NDSI combinations is thereby essential for validating the applicability of an NDSI for EO up-scaling
417 purposes.

418 The Dahra field site in Senegal, West Africa, was established in 2002 as an in situ research site to improve our
419 knowledge regarding properties of semi-arid savanna ecosystems and their responses to climatic and
420 environmental changes (Tagesson et al., 2015b). A strong focus of this instrumental setup is to gain insight into
421 the relationships between ground surface reflectance and savanna ecosystem properties for EO up-scaling
422 purposes. This paper presents a unique in situ dataset of seasonal dynamics in hyperspectral HCRF and

423 demonstrates how it can be used to describe the seasonal dynamics in ecosystem properties of semi-arid
424 savanna ecosystems. The objectives are threefold: (i) to quantify the relationship between seasonal dynamics
425 of in situ hyperspectral HCRF between 350 and 1800 nm and ecosystem properties (biomass, gross primary
426 productivity (GPP), LUE, and FAPAR); (ii) to quantify the relationship between NDSI with different wavelength
427 combinations (350 to 1800 nm) and the measured ecosystem properties; (iii) to analyse and quantify effects of
428 variable sun angles and sensor viewing geometries on different NDSI combinations.

429 **2. Materials and Method**

430 **2.1 Site description**

431 All measurements used for the present study were conducted at the Dahra field site in the Sahelian
432 ecoclimatic zone north-east of the town Dahra in the semi-arid central part of Senegal (15°24'10"N,
433 15°25'56"W) during 2011 and 2012 (Fig. 1). Rainfall is sparse in the region with a mean annual sum of
434 416 mm (1951-2003). More than 95% of the rain falls between July and October, with August being
435 the wettest month. The mean annual air temperature is 29 °C (1951-2003), May is the warmest and
436 January is the coldest month with mean monthly temperature of 32°C and 25°C, respectively. The
437 Dahra site has a short growing season (~3 months), following the rainy season with leaf area index
438 generally ranging between 0 and 2 (Fensholt et al., 2004). South-western winds dominate during the
439 rainy season and north-eastern winds ~~dominate~~ during the dry season. The area is dominated by annual
440 grasses (e.g. *Schoenefeldia gracilis*, *Digitaria gayana*, *Dactyloctenium aegypticum*, *Aristida mutabilis*
441 and *Cenchrus biflorues*) (Mbow et al., 2013) and trees and shrubs (e.g. *Acacia senegalensis* and
442 *Balanites aegyptiaca*) are relatively sparse (~3% of the land cover) (Rasmussen et al., 2011). The
443 average tree height was 5.2 m and the peak height of the herbaceous layer was 0.7 m (Tagesson et al.,
444 2015b). A thorough description of the Dahra field site is given in Tagesson et al. (2015b).

445 <Figure 1>

446 **2.2 Meteorological and vegetation variables**

447 A range of meteorological variables have been measured in a tower at the Dahra field site for more than ten
448 years: air temperature (°C) and relative humidity (%) were measured at 2 m height; soil temperature (°C) and
449 soil moisture (volumetric water content ($\text{m}^3 \text{m}^{-3} \times 100$) (%)) were collected at 0.05m depths; rainfall (mm) was
450 measured at 2 m height; incoming ($_{inc}$) and reflected ($_{ref}$) PAR ($\mu\text{mol m}^{-2} \text{s}^{-1}$) was measured at 10.5 m height, and
451 PAR transmitted through the vegetation ($\text{PAR}_{transmit}$) was measured at 6 plots at ~ 0.01 m height (Table 1)
452 (Tagesson et al., 2015b). The $\text{PAR}_{transmit}$ was measured within 7 meters distance from the tower. PAR absorbed
453 by the vegetation (APAR) was estimated by:

$$454 \quad \text{APAR} = \text{PAR}_{inc} - \text{PAR}_{ref} - (1 - \alpha_{soil}) \times \text{PAR}_{transmit}$$

455 (1)

456 where α_{soil} is the PAR albedo of the soil, which was measured as 0.20 (Tagesson et al., 2015b). FAPAR was
457 estimated by dividing APAR with PAR_{inc} (Tagesson et al., 2015b). All sensors were connected to a CR-1000
458 logger in combination with a multiplexer (Campbell Scientific Inc., North Logan, USA). ~~D-and~~ data were sampled
459 every 30 s, and stored as 15 minute averages (sum for rainfall).

460 The total above ground green biomass (g m^{-2}) of the herbaceous vegetation was sampled approximately
461 every 10 days during the growing seasons 2011 and 2012 at 28 one m^2 plots located along two ~ 1060 m long
462 diagonal transects (Fig. 1f) (Mbow et al., 2013). The method applied was destructive, so even though the same
463 transects were used for each sampling date, the plots were never positioned at exactly the same location. The
464 study area is flat and characterised by homogenous grassland savanna and the conditions in these sample plots
465 are generally found to be representative for the conditions in the entire measurement area (Fensholt et al.,

466 2006). All above ground green herbaceous vegetation matter was collected and weighed in the field to get the
467 fresh weight. The dry matter (DW) was estimated by oven-drying the green biomass. For a thorough
468 description regarding the biomass sampling we refer to Mbow et al. (2013).

469 <Table 1>

470 **2.3 Estimates of gross primary productivity and light use efficiency**

471 Net ecosystem exchange of CO₂ (NEE) ($\mu\text{mol CO}_2 \text{ m}^{-2} \text{ s}^{-1}$) was measured with an eddy covariance system,
472 consisting of an open path infrared gas analyser (LI-7500, LI-COR Inc., Lincoln, USA) and a 3-axis sonic
473 anemometer (Gill instruments, Hampshire, UK) from 18 July 2011 until 31 December 2012 (Table 1). The
474 sensors were mounted 9 m above the ground on a tower (placed 50 m south of the tower including the
475 meteorological and spectroradiometric sensors) (Fig. 1f). Data were sampled at 20 Hz rate. The post-processing
476 was done with the EddyPro 4.2.1 software (LI-COR Biosciences, 2012), and statistics were calculated for 30
477 minute periods. The post-processing includes 2-D coordinate rotation (Wilczak et al., 2001), time lag removal
478 between anemometer and gas analyser by covariance maximization (Fan et al., 1990), despiking (Vickers and
479 Mahrt, 1997) (plausibility range: window average ± 3.5 standard deviations), linear detrending (Moncrieff et al.,
480 2004), and compensation for density fluctuations (Webb et al., 1980). Fluxes were also corrected for high pass
481 (Moncrieff et al., 1997) and low pass filtering effects (Moncrieff et al., 2004). The data were filtered for steady
482 state and fully developed turbulent conditions, following Foken et al. (2004), and according to statistical tests
483 as recommended by Vickers and Mahrt (1997). Flux measurements from periods of heavy rainfall were also
484 removed. For a thorough description of the post processing of the raw eddy covariance data, see Tagesson et
485 al. (2015a).

486 A possible source of error in a comparison between EC-based variables and spectral HCRF is the difference in
487 footprint in footprint/ instantaneous field of view (IFOV) between the sensors. The IFOV of the

488 spectroradiometer set-up contains only soil and herbaceous vegetation. The footprint of the EC tower was
 489 estimated using a model based on measurement height, surface roughness and atmospheric stability (Hsieh et
 490 al., 2000). The median point of maximum contribution is at 69 m, and the median 70% cumulative flux distance
 491 is at 388 m from the tower. The footprint of the EC tower ~~contains~~semiconains semi-arid savanna grassland
 492 with ~3% tree coverage and the EC data is thereby affected by both woody and herbaceous vegetation (Fig. 1a
 493 and 1f). But given the low tree coverage, and the dominant influence of herbaceous vegetation on the
 494 seasonal dynamics in CO₂ fluxes, we still consider it ~~reasonable~~reasonable to compare EC fluxes with seasonal
 495 dynamics in spectral HCRF of the herbaceous vegetation.

496 The daytime NEE was partitioned to GPP and ecosystem respiration using the Mitscherlich light response
 497 function against PAR_{inc} (Falge et al., 2001). A 7-day moving window with one day time steps was used when
 498 fitting the functions. By subtracting dark respiration (R_d) from the light response function, it was forced through
 499 0, and GPP was estimated:

$$500 \quad GPP = -(F_{csat} + R_d) \times \left(1 - e^{\left(\frac{-\alpha \times PAR_{inc}}{F_{csat} + R_d}\right)}\right)$$

501 (2)

502 where F_{csat} is the CO₂ uptake at light saturation (μmol CO₂ m⁻² s⁻¹), and α is the quantum efficiency or the initial
 503 slope of the light response curve (μmol CO₂ (μmol photons)⁻¹) (Falge et al., 2001). Vapour pressure deficit (VPD)
 504 limits GPP and to account for this effect, the F_{csat} parameter was set as an exponentially decreasing function:

$$505 \quad F_{csat} = \begin{cases} F_{csat} \times e^{-k(VPD - VPD_0)} & VPD > VPD_0 \\ F_{csat} & VPD < VPD_0 \end{cases} \quad (3)$$

506 where VPD₀ is 10 hPa following the method by Lasslop et al. (2010).

507 Gaps in GPP less or equal to three days were filled with three different methods: (i) gaps shorter than
508 two hours were filled using linear interpolation; (ii) daytime gaps were filled by using the light-
509 response function for the 7-day moving windows; (iii) remaining gaps were filled by using mean
510 diurnal variation 7-days moving windows (Falge et al., 2001). A linear regression model was fitted
511 between daytime GPP and APAR for each 7-day moving window to estimate LUE, where LUE is the
512 slope of the line.

513 **2.4 Hyperspectral HCRF measurements and NDSI estimates**

514 Ground surface HCRF spectra were measured every 15 minutes between sunrise and sunset from 15 July 2011
515 until 31 December 2012 using two FieldSpec3 spectrometers with fiber optic cables (Table 1) (ASD Inc.,
516 Colorado, USA). The spectroradiometers cover the spectral range from 350 nm to 1800 nm and have a FOV of
517 25°. The spectral resolution is 3 nm at 350-1000 nm and 10 nm at 1000-1800 nm and the sampling interval is
518 1.4 nm at 350-1000 nm and 2 nm at 1000-1800 nm. From these data, 1 nm spectra were calculated by using
519 cubic spline interpolation functions. One sensor head was mounted on a rotating head 10.5 m above the
520 surface (at the same tower including instruments to measure meteorological variables) providing
521 measurements of the herbaceous vegetation from seven different viewing angles in a transect underneath the
522 tower (nadir, 15°, 30°, 45° off-nadir angles towards east and west). No trees or effects of shading of trees are
523 present in the IFOV of the data used in this study (Fig. 1). A reflective cosine receptor is used to measure full-
524 sky-irradiance by having the second sensor head mounted on a 2 m high stand pointing to a Spectralon panel
525 (Labsphere Inc., New Hampshire, USA) under a glass dome.

526 Each sensor measurement starts with an optimization to adjust the sensitivity of the detectors according to
527 the specific illumination conditions at the time of measurement. The optimisation is followed by a dark current
528 measurement to account for the noise generated by the thermal electrons within the ASDs that flows even

529 when no photons are entering the device. The measurement sequence starts with a full-sky-irradiance
530 measurement, followed by measurements of the 7 angles of the land surface and finalized by a second full-sky-
531 irradiance measurement. Thirty scans are averaged to one measurement to improve the signal-to-noise ratio
532 for each measurement (optimisation, dark current, full-sky irradiance and each of the seven target
533 measurements). The full measurement sequence takes less than one minute. The two ASD instruments are
534 calibrated against each other before and after each rainy season. Poor quality measurements caused by
535 ~~unfavorable~~unfavourable weather conditions, changing illumination conditions, irregular technical issues were
536 filtered by comparing full-sky solar irradiance before and after the target measurements (Huber et al., 2014).
537 The spectral HCRF was derived by estimating the ratio between the ground surface radiance and full sky
538 irradiance. For a complete description/illustration of the spectroradiometer set up, the measurement sequence
539 and the quality control, see Huber et al. (2014).

540 NDSI using all possible combinations of two separate wavelengths were calculated as:

$$541 \quad \text{NDSI} = \frac{(\rho_i - \rho_j)}{(\rho_i + \rho_j)}$$

542 (4)

543 where ρ_i and ρ_j are the daily median HCRF in two separate single wavelengths (i and j) between 350 and 1800
544 nm. In order to minimise the influence of errors we used daily median hyperspectral HCRF in the analysis (since
545 median provides the most common model output and is thereby more robust against outliers than average
546 values). ~~NDSI including the water absorption band (1300–1500 nm) was removed~~filtered as it is strongly
547 sensitive to atmospheric water content, and is less suitable for spatial extrapolation of ecosystem properties
548 using air/space borne sensors (Asner, 1998). Finally, NDSI combinations including wavelengths between 350
549 and 390 nm were filtered owing to low signal to noise ratio in the ASD sensors (Thenkabail et al., 2004).

550 **2.5 Effects of varying sun and sensor viewing geometry on NDSI**

551 The effects of variable solar zenith angles on different NDSI combinations were studied with nadir
552 HCRF measurements. In order to capture the seasonal dynamics, data were taken over 15 days during
553 four periods: 1) the dry season in 2012 (day of year (DOY) 71-85), 2) the fast growth period in 2011
554 (start of the rainy season) (DOY 200-214), 3) the peak of the growing season in 2011 (day-of-year DOY
555 237-251), and 4) the senescent period in 2011 (the end of the rainy season) (DOY 278-293). Only days
556 with full data coverage were used (~~12 of the 15 days~~) in order not to include bias in the results from
557 days with incomplete datasets. The median HCRF of the 15 days was calculated for each wavelength
558 for every 15 minutes between 8:00 and 18:00 (UTC). These HCRF values were combined into NDSI
559 with different wavelength combinations. Finally, daily mean and standard deviation for all wavelength
560 combinations were calculated. Diurnal variability in the NDSI was assessed with the coefficient of
561 variation (COV), which is the ratio between the standard deviation and the mean. The COV gives an
562 indication of effects related to variable solar zenith angles.

563 To capture directional effects in the NDSI related to the variable view zenith angles (15°, 30°, 45°
564 off-nadir angles towards east and west) the NDSI was calculated using median HCRF values from the
565 peak of the growing season 2011 (day of year 237-251)-four above-mentioned periods for the different
566 viewing angles. Only data measured between 12:00 and 14:00 (UTC) was used to avoid effects of
567 variable solar zenith angles. The anisotropy factor (ANIF) is defined as the fraction of a reflected
568 property at a specific view direction relative to the nadir, and it was calculated by:

569
$$\text{ANIF}(\lambda, \theta) = \frac{\text{NDSI}(\lambda, \theta)}{\text{NDSI}_0(\lambda)}$$

570 (5)

571 where $NDSI(\lambda, \theta)$ is NDSI for the different wavelengths (λ) and the different viewing angles (θ), and $NDSI_0(\lambda)$ is
572 the nadir measured NDSI (Sandmeier et al., 1998).

573 **2.6 Relationship between hyperspectral HCRF, NDSI and ecosystem properties**

574 We examined the relationship between predictor variables (daily median hyperspectral HCRF, and NDSI from
575 nadir observations) and response variables (biomass, GPP, LUE, and FAPAR) ~~using linear regression analysis. A~~
576 comparison between fitted linear and exponential regression models indicated no improvement by fitting
577 exponential regression models; we hence choose to use linear regression analysis (Supplementary material).

578 Possible errors (random sampling errors, aerosols, dust or water on the sensor heads, electrical sensor noise,
579 filtering and gap-filling errors, errors in correction factors, sensor drift, and instrumentation errors) can be
580 present in predictor and response variables. We thereby used a reduced major axis linear regression to account
581 for errors in both the predictor and response variables when fitting the regression lines. In order to estimate
582 the robustness of the empirical relationships, we used a bootstrap simulation methodology, where the
583 datasets were copied 200 times (Richter et al., 2012). The runs generated 200 sets of slopes, intercepts,
584 coefficients of determination (R^2), from which median and standard deviation was estimated. The generated
585 statistical models were validated against the left-out subsamples within the bootstrap simulation method by
586 calculating the root-mean square error (RMSE) and the relative RMSE ($RRMSE=100*RMSE*\text{mean}(\text{observed})^{-1}$);
587 median and standard deviation were estimated. Within the regression analysis all variables used were
588 repeated observations of the same measurement plot. The dependent and independent variables are
589 therebyhence temporally auto-correlated and cannot be regarded as statistically independent. We thereby
590 choose not to present any statistical significance. The analyses, however, still indicate how closely coupled the
591 explanatory variables are with the ecosystem properties.

592 A filter was created for the analysis between NDSI and ecosystem properties; all NDSI combinations with a
593 COV higher than 0.066 in any of the four periods (dry season, fast growth period, peak of the growing season,
594 and senescent period) and all NDSI combinations with ANIF values higher than 1.2 and lower than 0.8 in any of
595 the four periods were filtered. The ANIF thresholds of 1.2 and 0.8, and the COV threshold of 0.066 was used
596 since values then vary less than 20% due to effects of variable sun-sensor geometry. NDSI including the water
597 absorption band (1300-1500 nm) was also removed as it is strongly sensitive to atmospheric water content,
598 and is less suitable for spatial extrapolation of ecosystem properties using air/space borne sensors (Asner,
599 1998). Finally, NDSI combinations including wavelengths between 350 and 390 nm were removed owing to low
600 signal to noise ratio in the ASD sensors (Thenkabail et al., 2004).

601 3. Results

602 3.1 Seasonal dynamics in meteorological variables, ecosystem properties and 603 hyperspectral HCRF

604 Daily average air temperature at 2 m height ranged between 18.4°C and 37.8°C, with low values during
605 winter and peak values at the end of the dry season (Fig. 2a). Yearly rainfall was 486 mm and 606 mm
606 for 2011 and 2012, respectively. Soil moisture ranged between 1.9% and 14.1%, and it clearly followed
607 the rainfall patterns (Fig. 2b and 2c). The CO₂ fluxes were low during the dry period and high during
608 the rainy season (July-October) (Fig. 2e). The LUE followed GPP closely (Fig. 2f). FAPAR was low at
609 the start of the rainy season, followed by a maximum towards the end of the rainy season, and then
610 slowly decreased over the dry season (Fig. 2g).

611 The range in HCRF is large across the spectral space, and would hide the seasonal dynamics in hyperspectral
612 HCRF if directly shown. Therefore, to clearly illustrate the se seasonal dynamics in hyperspectral HCRF, the ratio
613 between daily median nadir HCRF and the average HCRF for the entire measurement period was calculated for
614 each wavelength (350-1800 nm). This gives a fraction of how the HCRF for each wavelength varies over the

615 measurement period in relation to the average of the entire period (Fig. 2d). In the visible (VIS) part of the
616 spectrum (350-700 nm) there was a stronger absorption during the second half of the rainy season and at the
617 beginning of the dry season than during the main part of the dry season and the start of the rainy season.
618 There was stronger NIR absorption (700-1300 nm) at the end of the rainy season and the beginning of the dry
619 season, whereas the absorption decreased along with the dry season. Strong seasonal variation was observed
620 in the water absorption region around 1400 nm following the succession of rainy and dry seasons. HCRF in the
621 short-wave infrared (SWIR; 1400-1800 nm) generally followed the seasonal dynamics of the visible part of the
622 spectrum.

623 <Figure 2>

624 3.2 Effects of sensor viewing geometry and variable sun angles on NDSI

625 The ~~most pronounced~~strongest effects of solar zenith angles and variable viewing geometry on NDSI
626 ~~at the peak of the growing season 2011~~ were observed at the peak of the growing season 2011 (Fig. 3,
627 Fig 4, and Fig S1-S5 in Supplementary material). In the main paper, we hence choose to present the
628 figures from this period; figures from remaining periods are located in supplementary material. The
629 most pronounced effects of solar zenith angles were observed for NDSI combining SWIR and NIR
630 wavelengths, and with VIS wavelengths between 550 nm and 700 nm (n=576) (Fig. 3). ~~Remaining VIS~~
631 ~~wavelengths were mostly affected by solar zenith angles when combined with the water absorption~~
632 ~~wavelengths around 1400 nm.~~ The same effects were seen for the view zenith angles; the strongest
633 effects were seen for NDSI with SWIR and NIR combinations, and VIS wavelengths between 550 and
634 700 nm (Fig. 4). Remaining VIS wavelengths were less affected. It was also clear that ground surface
635 anisotropy increased strongly as a function of increasing viewing angle (Fig. 4). Moreover, some band
636 combinations showed already angular sensitivity at view zenith angles of 15 °, while other band

637 combinations only manifest anisotropic behaviour with higher view angles. Some band combinations,
638 however, do not show any increased anisotropy at all (areas coloured in green in all ~~three-six~~ plots).
639 <Figure 3>
640 <Figure 4>

641 3.3 Relationship between hyperspectral HCRF, NDSI and ecosystem properties

642 3.3.1 Biomass

643 HCRF values for all wavelengths except the water absorption band at 1100 nm were strongly correlated to
644 biomass (Fig. 5a). The strongest correlation was found at ρ_{1675} (median \pm 1standard deviation; $r=-0.88\pm 0.09$),
645 but biomass was almost equally well correlated to blue, red and NIR wavelengths. All presented correlations
646 and relationships throughout the text are based on filtered data. Negative correlations indicate that the more
647 biomass the higher the absorption and hence the lower the HCRF. A small peak of positive correlation is seen at
648 1120-1150 nm ~~caused by a water absorption peak around this wavelength (Thenkabail et al., 2012)~~. NDSI
649 combinations with HCRF in the red edge ($\rho_{680}-\rho_{750}$) and HCRF in the VIS region explained seasonal dynamics in
650 biomass well (Fig. 6a). The strongest relationship ($R^2=0.88\pm 0.07$; RRMSE=18.6 \pm 5.7%) ~~between~~ between NDSI
651 and biomass was found for NDSI combining 705 and 587 nm (NDSI[705, 587]) (Table 2, Fig. 7a).

652 3.3.2 Gross primary productivity

653 The relationship between GPP and nadir measured hyperspectral HCRF is inverted as compared to
654 other correlation coefficient lines (Fig. 5b), since GPP is defined as a withdrawal of CO₂ from the
655 atmosphere with higher negative values for a larger CO₂ uptake. The seasonal dynamics in GPP was
656 strongly positively correlated to HCRF in the blue, red, SWIR wavelengths, and the water absorption
657 band at 1100 nm whereas it was strongly negatively correlated to the NIR HCRF. The study revealed
658 the strongest positive and negative correlations for HCRF at 682 nm ($r=0.70\pm 0.02$) and 761 nm ($r=-$

659 0.74±0.02), respectively. NDSI combinations that explained most of the GPP variability were different
660 combinations of the VIS and NIR or red and SWIR wavelengths (Fig. 6b). However, the strongest
661 relationship was seen at NDSI[518, 556] ($R^2=0.86±0.02$; RRMSE=34.9±2.3%) (Table 2; Fig. 7b).

662 **3.3.3 Light use efficiency**

663 LUE was negatively correlated with HCRF in the blue, and red spectral ranges and in the water
664 absorption band at 1100 nm and it was positively correlated in the NIR wavelengths (Fig. 5c). HCRF at
665 761 nm yielded the strongest positive correlation ($r=0.87±0.01$). When combining the different
666 wavelengths to NDSI, the VIS wavelengths explained variation in LUE well, with the strongest
667 relationships in the red and blue parts of the spectrum (Fig. 6c). LUE correlated most strongly with
668 NDSI[436, 688] ($R^2=0.81±0.02$; RRMSE=52.8±3.8 %) (Table 2; Fig. 7c).

669 **3.3.4 Fraction of photosynthetically active radiation absorbed by the vegetation**

670 FAPAR was negatively correlated to nadir measured HCRF for most wavelengths (Fig. 5d); the higher
671 FAPAR the higher the absorption, and thereby the lower the HCRF. The strongest correlation was
672 found at a blue wavelength ρ_{412} ($r=-0.92±0.01$). When wavelengths were combined to NDSI,
673 combining violet/blue with NIR and SWIR wavelengths generated the NDSI with the strongest
674 relationships (Fig. 6d) with a maximum R^2 of 0.81±0.02 (RRMSE=14.6±0.7 %) for NDSI[399, 1295]
675 (Table 2; Fig. 7d).

676 <Table 2>

677 <Figure 5>

678 <Figure 6>

679 <Figure 7>

680 **4. Discussion**

681 **4.1 Effects of sensor viewing geometry and variable sun angles on the NDSI**

682 Effects of solar zenith angles and sensor viewing geometry were similar (Fig. 3 and 4), since they affect HCRF
683 measurements in a similar way (Kimes, 1983). In dense and erectophile canopies, HCRF increases with sensor
684 viewing and solar zenith angles, because a larger fraction of the upper vegetation canopy is
685 viewed/illuminated, whereas the shadowed lower part of the canopy contributes less to the measured signal as
686 shown previously by several studies (Huete et al., 1992; Jin et al., 2002; Huber et al., 2014; Kimes, 1983).
687 However, the radiative transfer within a green canopy is complex, and differs across the spectral region (Huber
688 et al., 2014). Less radiation is available for scattering of high absorbing spectral ranges (such as the VIS
689 wavelengths), and this tends to increase the contrast between shadowed and illuminated areas for these
690 wavelengths, whereas in the NIR and SWIR ranges, more radiation is scattered and transmitted, which thereby
691 decreases the difference between shadowed and illuminated areas within the canopy (Kimes, 1983; Hapke et
692 al., 1996). A recognised advantage of NDSI calculations is that errors/biases being similar in both wavelengths
693 included in the index are suppressed by the normalisation. However, for a given situation where errors/biases
694 are different for the wavelengths used, such as effects generated by sun-sensor geometry, it will affect the
695 value of the index. This was also the case at the Dahra field site: NDSI values were strongly affected at
696 wavelength combinations with large differences in effects of variable solar zenith angles (Fig. 6 in Huber et al.
697 (2014)) and ~~at wavelength combinations with large differences in effects related to the~~ variable view zenith
698 angles (Fig. 4 in Tagesson et al. (2015b)). This effect is especially pronounced in the case ~~for of~~ low index values
699 (closer to 0) whereas larger index values (closer to 1 and -1) become less sensitive. The relative HCRF difference
700 between NIR and SWIR is lower as compared to indices including the VIS domain; NIR/SWIR based indices
701 thereby generate lower NDSI values with higher sensitivity to sun-sensor geometry generated differences
702 between included wavelengths (Fig. 3 and 4). [This can also be seen in the SIWSI/NDVI comparison by Huber et](#)

703 [al \(2014\)](#);- SIWSI had large relative differences depending on viewing angle (~70%), whereas NDVI had relatively
704 [small \(~5%\) \(Fig. 10 in Huber et al. \(2014\)\)](#). Fensholt et al. (2010a) [showed the same to be true in a comparison](#)
705 [between SIWSI and NDVI based on MODIS data: SIWSI was insensitive to day-to-day variations in canopy water](#)
706 [status due to effects of solar zenith angles and sensor viewing geometry blurring the signal](#).

[A strong diurnal dynamic does not necessarily mean a poor NDSI. For example, the photochemical reflectance](#)
707 [index \(PRI\) was created for assessing diurnal dynamics in the xanthophyll cycle activity \(Gamon et al., 1992\)](#).
708 [Stomatal closure due to high temperatures could also influence diurnal dynamics of vegetation properties](#)
709 [\(Lasslop et al., 2010\), and hence the diurnal dynamics of NDSI. However, diurnal variation in reflectance caused](#)
710 [by diurnal variability in vegetation status is assumed minor in relation to the diurnal variability caused by](#)
711 [changes in solar zenith angles. Additionally, in our study we are interested in relationships in seasonal dynamics](#)
712 [of between the ecosystem properties and NDSI; diurnal variation can thereby interfere and introduce](#)
713 [uncertainty in such relationships](#).

715 The importance of directional effects for the applicability of normalized difference spectral indices has been
716 pointed out as an issue in numerous papers (e.g. Holben and Fraser, 1984; van Leeuwen et al., 1999; Cihlar et
717 al., 1994; Fensholt et al., 2010b; Gao et al., 2002). This study confirms these challenges for NIR/SWIR based
718 indices, but the results also indicate several wavelength combinations from which these effects are less severe
719 and potentially applicable to EO data without disturbance from viewing/illumination geometry for this type of
720 vegetation. Multi-angular HCRF data provide additional information of e.g. canopy structure, photosynthetic
721 efficiency and capacity (Bicheron and Leroy, 2000; Asner, 1998; Pisek et al., 2013; Huber et al., 2010), and this
722 unique in situ based multi-angular high temporal resolution dataset may thus be used for future research of
723 canopy radiative transfer and BRDF (bidirectional reflectance distribution function) modelling
724 (Jacquemoud et al., 2009; Bicheron and Leroy, 2000). The multi-angular dataset is also highly valuable for

725 evaluation and validation of satellite based products, where the separation of view angle and atmospheric
726 effects can only be done using radiative transfer models (Holben and Fraser, 1984).

727 **4.2 Seasonal dynamics in hyperspectral HCRF, NDSI and ecosystem properties**

728 **4.2.1 Biomass**

729 The strong correlation between biomass and most of the spectrum indicates the strong effects of phenology on
730 the seasonal dynamics in the HCRF spectra (Fig. 5a). Variability in VIS (350-700 nm) HCRF for vegetated areas is
731 strongly related to changes in leaf pigments (Asner, 1998), and this can also be seen in Fig. 2d since absorption
732 was much stronger during the rainy (growing) season, than during the dry season. Previous studies have
733 generally shown positive relationships between NIR HCRF and biomass since a large fraction of NIR radiation is
734 reflected in green healthy vegetation to avoid overheating (e.g. Hansen and Schjoerring, 2003; Asner, 1998).

735 Here, a strong negative relationship between NIR HCRF and dry weight biomass is generally observed (Fig. 5a),
736 indicating stronger NIR absorption with increased biomass. However, whereas a strong positive NIR HCRF
737 correlation with vegetation water content was seen (figure not shown). A possible explanation could be that
738 the sampled biomass at the end of the rainy season contained some senescent vegetation, and a correlation
739 against vegetation water content is hence closer to green healthy vegetation. This relationship is however
740 interesting and should be studied further to better understand the respective importance of canopy water and
741 leaf internal cellular structure for the NIR HCRF of herbaceous vegetation characterised by erectophile leaf
742 angle distribution (LAD) in semi-arid regions. We found the strongest correlation for biomass with a SWIR
743 wavelength thereby confirming the studies by Lee (2004) and Psomas et al. (2011) in that SWIR wavelengths
744 are good predictors of LAI or biomass.

745 The NDVI is known to saturate at high biomass ~~because the absorption of red light at ~680 nm saturates at~~
746 ~~higher biomass leads~~ because chlorophyll absorbs nearly all the red light at ~680 nm to the point where no

747 matter how much vegetation you add, more photons cannot be absorbed because they are already all
748 absorbed whereas the NIR HCRF continues to increase due to multiple scattering effects (Mutanga and
749 Skidmore, 2004; Jin and Eklundh, 2014). Several studies have shown that NDSI computed with narrowband
750 HCRF improve this relationship by choosing a wavelength region not as close to the maximum red absorption at
751 ~680 nm, for example using shorter and longer wavelengths of the red edge (700 - 780nm) (Cho et al., 2007;
752 Mutanga and Skidmore, 2004; Lee, 2004), and NIR and SWIR wavelengths (Psomas et al., 2011; Lee, 2004). The
753 NDSI with the strongest correlation to biomass was computed using red edge HCRF (ρ_{705}) and green HCRF (ρ_{587}).
754 Vegetation stress and information about chlorophyll and nitrogen status of plants can be extracted from the
755 red-edge region (Gitelson et al., 1996). Wavelengths around ρ_{550} are located right at the peak of green
756 reflection and closely related to the total chlorophyll content, leaf nitrogen content, and
757 chlorophyll/carotenoid ratio and have previously been shown to be closely related to biomass (Inoue et al.,
758 2008; Thenkabail et al., 2012).

759 **4.2.2 Gross primary productivity**

760 The maximum absorption in the red wavelengths generally occurs at 682 nm as this is the peak absorption for
761 chlorophyll a and b (Thenkabail et al., 2000), and this was also the wavelength being most strongly correlated
762 with GPP. HCRF at 682 nm was previously shown to be strongly related to LAI, biomass, plant height, NPP, and
763 crop type discrimination (Thenkabail et al., 2004; Thenkabail et al., 2012). The NDSI with the strongest
764 relationship to GPP was based on HCRF in the vicinity of the green peak. The photochemical reflectance index
765 (PRI) normalizes HCRF at 531 nm and 570 nm and it was suggested for detection of diurnal variation in the
766 xanthophyll cycle activity (Gamon et al., 1992), and it is commonly used for estimating productivity efficiency of
767 the vegetation (e.g. Soudani et al., 2014). The present study thereby confirms the strong applicability of the
768 wavelengths in the vicinity of the green peak for vegetation productivity studies. Again, wavelengths around

769 the green peak are related to the total chlorophyll content, leaf nitrogen content, chlorophyll/carotenoid ratio,
770 and biomass (Inoue et al., 2008; Thenkabail et al., 2012).

771 **4.2.3 Light use efficiency**

772 Both LUE and GPP were most strongly correlated with HCRF at 761 nm, which is the oxygen A-band within the
773 NIR wavelengths. HCRF at 761 nm is commonly used for estimating solar-induced chlorophyll fluorescence due
774 to radiation emitted by the chlorophyll, and it has been suggested as a direct measure of health status of the
775 vegetation (Meroni et al., 2009). Earth observation data for estimating fluorescence should have very high
776 spectral resolution (<10 nm) due to its narrow features, but considering the rapid technical development within
777 sensors for hyperspectral measurements, fluorescence possibly has strong practical potential for monitoring
778 vegetation status (Meroni et al., 2009; Entcheva Campbell et al., 2008). Globally mapped terrestrial chlorophyll
779 fluorescence retrievals are already produced from the GOME-2 instrument at a spatial resolution of 0.5°×0.5°,
780 but hopefully this will be available also with EO sensors of higher spatial and temporal resolution in the future
781 (Joiner et al., 2013).

782 The strongest wavelength combinations for estimating LUE for this semi-arid ecosystem was NDSI[688, 435].
783 The 688 nm wavelength is just at the base of the red edge region, again indicating the importance of this
784 spectral region for estimating photosynthetic activity. The wavelength at 435 nm is at the ~~center~~centre of the
785 blue range characterized by chlorophyll utilization, and strongly related to chlorophyll a and b, senescing,
786 carotenoid, loss of chlorophyll, and vegetation browning (Thenkabail et al., 2004; Thenkabail et al., 2012). The
787 NDSI[688, 435] thereby explores the difference between information about chlorophyll content and
788 information about senescence of the canopy, which should be a good predictor of ecosystem level
789 photosynthetic efficiency.

790 **4.2.4 Fraction of photosynthetically active radiation absorbed by the vegetation**

791 FAPAR is an estimate of radiation absorption in the photosynthetically active spectrum and thereby strongly
792 negatively correlated to most parts of the spectrum (Fig. 5d). FAPAR remained high during the dry season
793 because of standing dry biomass that was slowly degrading over the dry season (Fig. 2g). The seasonal
794 dynamics in FAPAR is thereby strongly related to senescence of the vegetation, which explains why FAPAR was
795 most strongly correlated to blue wavelengths (ρ_{412}). Several studies reported a strong relationship between
796 NDVI and FAPAR (e.g. Tagesson et al., 2012; Myneni and Williams, 1994; Fensholt et al., 2004), but this
797 relationship has been shown to vary for the vegetative phase and the periods of senescence (Inoue et al., 1998;
798 Tagesson et al., 2015b). As showed by Inoue et al. (2008), and confirmed by this study, new indices combining
799 blue with NIR wavelengths could be used for estimating FAPAR for the entire phenological cycle. This result has
800 implications for studies using the LUE approach for estimating C assimilations (Hilker et al., 2008).

801 **4.3 Outlook and perspectives**

802 Very limited multi-angular hyperspectral in situ data exists, even though it has been, and will continue to be
803 extremely valuable for an improved understanding of the interaction between ground surface properties and
804 radiative transfer. In this study, we have presented a unique in situ dataset of multi-angular, high temporal
805 resolution hyperspectral HCRF (350-1800 nm) and demonstrated the applicability of hyperspectral data for
806 estimating ground surface properties of semi-arid savanna ecosystems using NDSI. The study was conducted in
807 spatially homogeneous savanna grassland, suggesting that the results should be commonly applicable for this
808 biome type. However, attention should be paid to site-specific details that could affect the indices, such as
809 species composition, soil type, biotic and abiotic stresses, and stand structure. Additionally, the biophysical
810 mechanisms behind the NDSIs are not well understood at the moment, and further studies are needed to
811 examine the applicability of these indices to larger regions and other ecosystems. Being a 2-band ratio
812 approach, NDSI does not take full advantage of exploring the rich information given by the hyperspectral HCRF

813 measurements. In the future, this hyperspectral HCRF data-set could be fully explored using e.g.
814 derivative techniques, multivariate methods, and creation, parameterisation and evaluation of BRDF
815 and radiative transfer models.

816 Even though several other methods exist which fully exploit the information in the hyperspectral spectrum,
817 results of the present study still indicate the strength of normalised difference indices for extrapolating
818 seasonal dynamics in properties of savanna ecosystems. A number of wavelengths spectra that are highly
819 correlated to seasonal dynamics in properties of semiarid savanna ecosystems have been identified. The
820 relationships between NDSI and ecosystem properties were better determined, or at the same level, as results
821 of previous studies exploring relationships between hyperspectral reflectance and ecosystem properties
822 (Kumar, 2007; Cho et al., 2007; Mutanga and Skidmore, 2004; Psomas et al., 2011; Ide et al., 2010). By
823 studying also the impact from varying viewing and illumination geometry the feasibility and applicability of
824 using indices for up-scaling to EO data was evaluated. As such, the results presented here offer insights for
825 assessment of ecosystem properties using EO data and this information could be used for designing future
826 sensors for observation of ecosystem properties of the Earth.

827 **Acknowledgements**

828 This paper was written within the frame of the project entitled Earth Observation based Vegetation
829 productivity and Land Degradation Trends in Global Drylands. The project was funded by the Danish
830 Council for Independent Research (DFF) Sapere Aude programme. The site is maintained by the
831 Centre de Recherches Zootechniques de Dahra, Institut Sénégalais de Recherches Agricoles (ISRA).

832

833

834 **References**

- 835 Asner, G. P.: Biophysical and Biochemical Sources of Variability in Canopy Reflectance, *Remote Sens.*
836 *Environ.*, 64, 234-253, [http://dx.doi.org/10.1016/S0034-4257\(98\)00014-5](http://dx.doi.org/10.1016/S0034-4257(98)00014-5), 1998.
- 837 Bicheron, P., and Leroy, M.: Bidirectional reflectance distribution function signatures of major biomes
838 observed from space, *J. Geophys. Res. -Atmos.*, 105, 26669-26681, 10.1029/2000JD900380, 2000.
- 839 Bowyer, P., and Danson, F. M.: Sensitivity of spectral reflectance to variation in live fuel moisture
840 content at leaf and canopy level, *Remote Sens. Environ.*, 92, 297-308,
841 <http://dx.doi.org/10.1016/j.rse.2004.05.020>, 2004.
- 842 Ceccato, P., Gobron, N., Flasse, S., Pinty, B., and Tarantola, S.: Designing a spectral index to estimate
843 vegetation water content from remote sensing data: Part 1: Theoretical approach, *Remote Sens.*
844 *Environ.*, 82, 188-197, [http://dx.doi.org/10.1016/S0034-4257\(02\)00037-8](http://dx.doi.org/10.1016/S0034-4257(02)00037-8), 2002.
- 845 Cho, M. A., Skidmore, A., Corsi, F., van Wieren, S. E., and Sobhan, I.: Estimation of green grass/herb
846 biomass from airborne hyperspectral imagery using spectral indices and partial least squares
847 regression, *Int. J. Appl. Earth Obs. Geoinf.*, 9, 414-424, <http://dx.doi.org/10.1016/j.jag.2007.02.001>,
848 2007.
- 849 Cihlar, J., Manak, D., and Voisin, N.: AVHRR bidirectional reflectance effects and compositing, *Remote*
850 *Sens. Environ.*, 48, 77-88, [http://dx.doi.org/10.1016/0034-4257\(94\)90116-3](http://dx.doi.org/10.1016/0034-4257(94)90116-3), 1994.
- 851 Coburn, C. A., and Peddle, D. R.: A low-cost field and laboratory goniometer system for estimating
852 hyperspectral bidirectional reflectance, *Can. J. Remote Sens.*, 32, 244-253, 10.5589/m06-021, 2006.
- 853 Danson, F. M., Steven, M. D., Malthus, T. J., and Clark, J. A.: High-spectral resolution data for
854 determining leaf water content, *Int. J. Remote Sens.*, 13, 461-470, 10.1080/01431169208904049,
855 1992.
- 856 Entcheva Campbell, P. K., Middleton, E. M., Corp, L. A., and Kim, M. S.: Contribution of chlorophyll
857 fluorescence to the apparent vegetation reflectance, *Sci. Total Environ.*, 404, 433-439,
858 <http://dx.doi.org/10.1016/j.scitotenv.2007.11.004>, 2008.
- 859 Falge, E., Baldocchi, D., Olson, R., Anthoni, P., Aubinet, M., Bernhofer, C., Burba, G., Ceulemans, R.,
860 Clement, R., Dolman, H., Granier, A., Gross, P., Grunwald, T., Hollinger, D., Jensen, N. O., Katul, G.,
861 Keronen, P., Kowalski, A., Lai, C. T., Law, B. E., Meyers, T., Moncrieff, J., Moors, E., Munger, J. W.,
862 Pilegaard, K., Rannik, U., Rebmann, C., Suyker, A., Tenhunen, J., Tu, K., Verma, S., Vesala, T., Wilson,
863 K., and Wofsy, S.: Gap filling strategies for defensible annual sums of net ecosystem exchange, *Agric.*
864 *For. Meteorol.*, 107, 43-69, 2001.
- 865 Fan, S. M., Wofsy, S. C., Bakwin, P. S., Jacob, D. J., and Fitzjarrald, D. R.: Atmosphere-Biosphere
866 Exchange of CO₂ and O₃ in the Central Amazon Forest, *J. Geophys. Res.*, 95, 16851-16864, 1990.
- 867 Fensholt, R., Sandholt, I., and Rasmussen, M. S.: Evaluation of MODIS LAI, fAPAR and the relation
868 between fAPAR and NDVI in a semi-arid environment using in situ measurements, *Remote Sens.*
869 *Environ.*, 91, 490-507, <http://dx.doi.org/10.1016/j.rse.2004.04.009>, 2004.
- 870 Fensholt, R., Sandholt, I., and Stisen, S.: Evaluating MODIS, MERIS, and VEGETATION vegetation
871 indices using in situ measurements in a semiarid environment, *IEEE T. Geosci. Remote*, 44, 1774-1786,
872 10.1109/TGRS.2006.875940, 2006.

873 Fensholt, R., Huber, S., Proud, S. R., and Mbow, C.: Detecting Canopy Water Status Using Shortwave
874 Infrared Reflectance Data From Polar Orbiting and Geostationary Platforms, *IEEE J. Sel. Top. Appl.*, 3,
875 271-285, [10.1109/jstars.2010.2048744](https://doi.org/10.1109/jstars.2010.2048744), 2010a.

876 Fensholt, R., Sandholt, I., Proud, S. R., Stisen, S., and Rasmussen, M. O.: Assessment of MODIS sun-
877 sensor geometry variations effect on observed NDVI using MSG SEVIRI geostationary data, *Int. J.*
878 *Remote Sens.*, 31, 6163-6187, 2010b.

879 Feret, J.-B., François, C., Asner, G. P., Gitelson, A. A., Martin, R. E., Bidel, L. P. R., Ustin, S. L., le Maire,
880 G., and Jacquemoud, S.: PROSPECT-4 and 5: Advances in the leaf optical properties model separating
881 photosynthetic pigments, *Remote Sens. Environ.*, 112, 3030-3043,
882 <http://dx.doi.org/10.1016/j.rse.2008.02.012>, 2008.

883 Foken, T., Gøckede, M., Mauder, M., Mahrt, L., Amiro, B., and Munger, W.: Post-field data quality
884 control, in: *Handbook of Micrometeorology- A guidebook for Surface Flux Measurement and Analysis*,
885 edited by: Lee, J. A., Massman, W., and Law, B., Kluwer Academic Publishers, London, 181-203, 2004.

886 Gamon, J. A., Peñuelas, J., and Field, C. B.: A narrow-waveband spectral index that tracks diurnal
887 changes in photosynthetic efficiency, *Remote Sens. Environ.*, 41, 35-44,
888 [http://dx.doi.org/10.1016/0034-4257\(92\)90059-S](http://dx.doi.org/10.1016/0034-4257(92)90059-S), 1992.

889 Gao, F., Jin, Y., Schaaf, C. B., and Strahler, A. H.: Bidirectional NDVI and atmospherically resistant BRDF
890 inversion for vegetation canopy, *IEEE T. Geosci. Remote*, 40, 1269-1278, [10.1109/TGRS.2002.800241](https://doi.org/10.1109/TGRS.2002.800241),
891 2002.

892 Gates, D. M., Keegan, H. J., Schleter, J. C., and Weidner, V. R.: Spectral Properties of Plants, *Appl.*
893 *Optics*, 4, 11-20, 1965.

894 Gitelson, A. A., Merzlyak, M. N., and Lichtenthaler, H. K.: Detection of Red Edge Position and
895 Chlorophyll Content by Reflectance Measurements Near 700 nm, *J. Plant Physiol.*, 148, 501-508,
896 [http://dx.doi.org/10.1016/S0176-1617\(96\)80285-9](http://dx.doi.org/10.1016/S0176-1617(96)80285-9), 1996.

897 Gower, S. T., Kucharik, C. J., and Norman, J. M.: Direct and indirect estimation of leaf area index,
898 fAPAR, and net primary production of terrestrial ecosystems - a real or imaginary problem?, *Remote*
899 *Sens. Environ.*, 70, 29-51, 1999.

900 Hansen, P. M., and Schjoerring, J. K.: Reflectance measurement of canopy biomass and nitrogen
901 status in wheat crops using normalized difference vegetation indices and partial least squares
902 regression, *Remote Sens. Environ.*, 86, 542-553, [http://dx.doi.org/10.1016/S0034-4257\(03\)00131-7](http://dx.doi.org/10.1016/S0034-4257(03)00131-7),
903 2003.

904 Hapke, B., DiMucci, D., Nelson, R., and Smythe, W.: The cause of the hot spot in vegetation canopies
905 and soils: Shadow-hiding versus coherent backscatter, *Remote Sens. Environ.*, 58, 63-68,
906 [http://dx.doi.org/10.1016/0034-4257\(95\)00257-X](http://dx.doi.org/10.1016/0034-4257(95)00257-X), 1996.

907 Hilker, T., Coops, N. C., Nestic, Z., Wulder, M. A., and Black, A. T.: Instrumentation and approach for
908 unattended year round tower based measurements of spectral reflectance, *Comput. Electron. Agr.*,
909 56, 72-84, [10.1016/j.compag.2007.01.003](https://doi.org/10.1016/j.compag.2007.01.003), 2007.

910 Hilker, T., Coops, N. C., Wulder, M. A., Black, T. A., and Guy, R. D.: The use of remote sensing in light
911 use efficiency based models of gross primary production: A review of current status and future
912 requirements, *Sci. Total Environ.*, 404, 411-423, <http://dx.doi.org/10.1016/j.scitotenv.2007.11.007>,
913 2008.

914 Hilker, T., Nestic, Z., Coops, N. C., and Lessard, D.: A new automated, multiangular radiometer
915 instrument for tower-based observations of canopy reflectance (AMSPEC II), *Instrum. Sci. Technol.*,
916 38, 319-340, 10.1080/10739149.2010.508357, 2010.

917 Holben, B., and Fraser, R. S.: Red and near-infrared sensor response to off-nadir viewing, *Int. J.*
918 *Remote Sens.*, 5, 145-160, 10.1080/01431168408948795, 1984.

919 Hsieh, C. I., Katul, G., and Chi, T. W.: An approximate analytical model for footprint estimation of
920 scalar fluxes in thermally stratified atmospheric flows, *Adv. Water Res.*, 23, 765-772, 2000.

921 Huber, S., Koetz, B., Psomas, A., Kneubuehler, M., Schopfer, J. T., Itten, K. I., and Zimmermann, N. E.:
922 Impact of multiangular information on empirical models to estimate canopy nitrogen concentration in
923 mixed forest, *APPRES*, 4, 043530-043530-043517, 10.1117/1.3435334, 2010.

924 Huber, S., Tagesson, T., and Fensholt, R.: An automated field spectrometer system for studying VIS,
925 NIR and SWIR anisotropy for semi-arid savanna, *Remote Sens. Environ.*, 152, 547–556, 2014.

926 Huete, A. R., Hua, G., Qi, J., Chehbouni, A., and van Leeuwen, W. J. D.: Normalization of
927 multidirectional red and NIR reflectances with the SAVI, *Remote Sens. Environ.*, 41, 143-154,
928 [http://dx.doi.org/10.1016/0034-4257\(92\)90074-T](http://dx.doi.org/10.1016/0034-4257(92)90074-T), 1992.

929 Ide, R., Nakaji, T., and Oguma, H.: Assessment of canopy photosynthetic capacity and estimation of
930 GPP by using spectral vegetation indices and the light-response function in a larch forest, *Agric. For.*
931 *Meteorol.*, 150, 389-398, 2010.

932 Inoue, Y., Moran, M. S., and Horie, T.: Analysis of spectral measurements in rice paddies for predicting
933 rice growth and yield based on a simple crop simulation model, *Plant. Prod. Sci.*, 1, 269–279, 1998.

934 Inoue, Y., Penuelas, J., Miyata, A., and Mano, M.: Normalized difference spectral indices for estimating
935 photosynthetic efficiency and capacity at a canopy scale derived from hyperspectral and CO₂ flux
936 measurements in rice, *Remote Sens. Environ.*, 112, 156-172, 2008.

937 Jacquemoud, S., Verhoef, W., Baret, F., Bacour, C., Zarco-Tejada, P. J., Asner, G. P., François, C., and
938 Ustin, S. L.: PROSPECT+SAIL models: A review of use for vegetation characterization, *Remote Sens.*
939 *Environ.*, 113, Supplement 1, S56-S66, <http://dx.doi.org/10.1016/j.rse.2008.01.026>, 2009.

940 Javier García-Haro, F., Camacho-de Coca, F., and Meliá, J.: Retrieving leaf area index from multi-
941 angular airborne data, *Ann. Geophys.*, 49, 209-218, 2006.

942 Jin, H., and Eklundh, L.: A physically based vegetation index for improved monitoring of plant
943 phenology, *Remote Sens. Environ.*, 152, 512-525, <http://dx.doi.org/10.1016/j.rse.2014.07.010>, 2014.

944 Jin, Y., Gao, F., Schaaf, C. B., Xiaowen, L., Strahler, A. H., Bruegge, C. J., and Martonchik, J. V.:
945 Improving MODIS surface BRDF/Albedo retrieval with MISR multiangle observations, *IEEE T. Geosci.*
946 *Remote*, 40, 1593-1604, 10.1109/TGRS.2002.801145, 2002.

947 Joiner, J., Guanter, L., Lindstrot, R., Voigt, M., Vasilkov, A. P., Middleton, E. M., Huemmrich, K. F.,
948 Yoshida, Y., and Frankenberg, C.: Global monitoring of terrestrial chlorophyll fluorescence from
949 moderate-spectral-resolution near-infrared satellite measurements: methodology, simulations, and
950 application to GOME-2, *Atmospheric Measuring Techniques*, 6, 2803-2823, doi:10.5194/amt-6-2803-
951 2013, 2013.

952 Kimes, D. S.: Dynamics of Directional Reflectance Factor Distributions for Vegetation Canopies, *Appl.*
953 *Optics*, 22, 1364-1372, 1983.

954 Kumar, L.: High-spectral resolution data for determining leaf water content in Eucalyptus species: leaf
955 level experiments, *Geocarto International*, 22, 3-16, 2007.

956 Lasslop, G., Reichstein, M., and Papale, D.: Separation of net ecosystem exchange into assimilation
957 and respiration using a light response curve approach: critical issues and global evaluation, *Global*
958 *Change Biol.*, 16, 187-209, 2010.

959 Laurent, V. C. E., Verhoef, W., Clevers, J. G. P. W., and Schaepman, M. E.: Inversion of a coupled
960 canopy–atmosphere model using multi-angular top-of-atmosphere radiance data: A forest case study,
961 *Remote Sens. Environ.*, 115, 2603-2612, <http://dx.doi.org/10.1016/j.rse.2011.05.016>, 2011.

962 Lee, K., Cohen, WB, Kennedy, RE, Maieringer, TK, Gower, ST Hyperspectral versus multispectral
963 data for estimating leaf area index in four different biomes, *Remote Sens. Environ.*, 91, 508-520, 2004.

964 Leuning, R., Hughes, D., Daniel, P., Coops, N. C., and Newnham, G.: A multi-angle spectrometer for
965 automatic measurement of plant canopy reflectance spectra, *Remote Sens. Environ.*, 103, 236-245,
966 10.1016/j.rse.2005.06.016, 2006.

967 LI-COR Biosciences: EDDYPRO Eddy Covariance Software Version 4.0 User's Guide & Reference, LI-COR
968 Inc., Lincoln, 200 pp., 2012.

969 Maignan, F., Bréon, F. M., and Lacaze, R.: Bidirectional reflectance of Earth targets: evaluation of
970 analytical models using a large set of spaceborne measurements with emphasis on the Hot Spot,
971 *Remote Sens. Environ.*, 90, 210-220, <http://dx.doi.org/10.1016/j.rse.2003.12.006>, 2004.

972 Martonchik, J. V., Bruegge, C. J., and Strahler, A. H.: A review of reflectance nomenclature used in
973 remote sensing, *Remote Sensing Reviews*, 19, 9-20, 10.1080/02757250009532407, 2000.

974 Mbow, C., Fensholt, R., Rasmussen, K., and Diop, D.: Can vegetation productivity be derived from
975 greenness in a semi-arid environment? Evidence from ground-based measurements, *J. Arid Environ.*,
976 97, 56-65, <http://dx.doi.org/10.1016/j.jaridenv.2013.05.011>, 2013.

977 Meroni, M., Rossini, M., Guanter, L., Alonso, L., Rascher, U., Colombo, R., and Moreno, J.: Remote
978 sensing of solar-induced chlorophyll fluorescence: Review of methods and applications, *Remote Sens.*
979 *Environ.*, 113, 2037-2051, <http://dx.doi.org/10.1016/j.rse.2009.05.003>, 2009.

980 Milton, E. J., Schaepman, M. E., Anderson, K., Kneubühler, M., and Fox, N.: Progress in field
981 spectroscopy, *Remote Sens. Environ.*, 113, Supplement 1, S92-S109,
982 <http://dx.doi.org/10.1016/j.rse.2007.08.001>, 2009.

983 Moncrieff, J. B., Massheder, J. M., de Bruin, H., Elbers, J., Friborg, T., Heusinkveld, B., Kabat, P., Scott,
984 S., Soegaard, H., and Verhoef, A.: A system to measure surface fluxes of momentum, sensible heat,
985 water vapour and carbon dioxide, *J. Hydrol.*, 188–189, 589-611, 10.1016/s0022-1694(96)03194-0,
986 1997.

987 Moncrieff, J. B., R. Clement, J. Finnigan, and Meyers, T.: Averaging, detrending and filtering of eddy
988 covariance time series, in: *Handbook of Micrometeorology: A Guide for Surface Flux Measurements*,
989 edited by: Lee, X., W. J., Massman and B. E. Law., Kluwer Academic, Dordrecht, 7-31, 2004.

990 Mutanga, O., and Skidmore, A. K.: Narrow band vegetation indices overcome the saturation problem
991 in biomass estimation, *Int. J. Remote Sens.*, 25, 3999-4014, 10.1080/01431160310001654923, 2004.

992 Myneni, R. B., and Williams, D. L.: On the relationship between FAPAR and NDVI, *Remote Sens.*
993 *Environ.*, 49, 200-211, 1994.

994 Pisek, J., Ryu, Y., Sprintsin, M., He, L., Oliphant, A. J., Korhonen, L., Kuusk, J., Kuusk, A., Bergstrom, R.,
995 Verrelst, J., and Alikas, K.: Retrieving vegetation clumping index from Multi-angle Imaging
996 SpectroRadiometer (MISR) data at 275 m resolution, *Remote Sens. Environ.*, 138, 126-133,
997 <http://dx.doi.org/10.1016/j.rse.2013.07.014>, 2013.

998 Psomas, A., Kneubühler, M., Huber, S., Itten, K., and Zimmermann, N. E.: Hyperspectral remote
999 sensing for estimating aboveground biomass and for exploring species richness patterns of grassland
1000 habitats, *Int. J. Remote Sens.*, 32, 9007-9031, 10.1080/01431161.2010.532172, 2011.

1001 Qi, J., Chehbouni, A., Huete, A. R., Kerr, Y. H., and Sorooshian, S.: A modified soil adjusted vegetation
1002 index, *Remote Sens. Environ.*, 48, 119-126, 1994.

1003 Rasmussen, M. O., Göttsche, F. M., Diop, D., Mbow, C., Olesen, F. S., Fensholt, R., and Sandholt, I.:
1004 Tree survey and allometric models for tiger bush in northern Senegal and comparison with tree
1005 parameters derived from high resolution satellite data, *Int. J. Appl. Earth Obs. Geoinf.*, 13, 517-527,
1006 10.1016/j.jag.2011.01.007, 2011.

1007 Richter, K., Atzberger, C., Hank, T. B., and Mauser, W.: Derivation of biophysical variables from Earth
1008 observation data: validation and statistical measures, *APPRES*, 6, 063557-063551-063557-063523,
1009 10.1117/1.JRS.6.063557, 2012.

1010 Roberto, C., Lorenzo, B., Michele, M., Micol, R., and Cinzini, P.: Optical Remote Sensing of Vegetation
1011 Water Content, in: *Hyperspectral Remote Sensing of Vegetation*, edited by: Thenkabail, P. S., Lyon, J.
1012 G., and Huete, A., CRC Press, Taylor and Francis Group, Boca Raton, FL, 227-244, 2012.

1013 Rouse, J. W., Haas, R. H., Schell, J. A., Deering, D. W., and Harlan, J. C.: Monitoring the Vernal
1014 Advancement of Retrogradation of Natural Vegetation, Type III, Final Report, Greenbelt, MD, 1974.

1015 Sandmeier, S., Müller, C., Hosgood, B., and Andreoli, G.: Physical Mechanisms in Hyperspectral BRDF
1016 Data of Grass and Watercress, *Remote Sens. Environ.*, 66, 222-233, [http://dx.doi.org/10.1016/S0034-4257\(98\)00060-1](http://dx.doi.org/10.1016/S0034-4257(98)00060-1), 1998.

1018 Schaepman-Strub, G., Schaepman, M. E., Painter, T. H., Dangel, S., and Martonchik, J. V.: Reflectance
1019 quantities in optical remote sensing—definitions and case studies, *Remote Sens. Environ.*, 103, 27-42,
1020 <http://dx.doi.org/10.1016/j.rse.2006.03.002>, 2006.

1021 Schopfer, J., Dangel, S., Kneubühler, M., and Itten, K.: The Improved Dual-view Field Goniometer
1022 System FIGOS, *Sensors*, 8, 5120-5140, 2008.

1023 Sims, D. A., and Gamon, J. A.: Estimation of vegetation water content and photosynthetic tissue area
1024 from spectral reflectance: a comparison of indices based on liquid water and chlorophyll absorption
1025 features, *Remote Sens. Environ.*, 84, 526-537, 2003.

1026 Sjöström, M., Ardö, J., Eklundh, L., El-Tahir, B. A., El-Khidir, H. A. M., Hellström, M., Pilesjö, P., and
1027 Seaquist, J.: Evaluation of satellite based indices for gross primary production estimates in a sparse
1028 savanna in the Sudan, *Biogeosciences*, 6, 129-138, 2009.

1029 Soudani, K., Hmimina, G., Dufrêne, E., Berveiller, D., Delpierre, N., Ourcival, J.-M., Rambal, S., and
1030 Joffre, R.: Relationships between photochemical reflectance index and light-use efficiency in
1031 deciduous and evergreen broadleaf forests, *Remote Sens. Environ.*, 144, 73–84, 2014.

1032 Tagesson, T., Eklundh, L., and Lindroth, A.: Applicability of leaf area index products for boreal regions
1033 of Sweden, *Int. J. Remote Sens.*, 30, 5619–5632, 2009.

1034 Tagesson, T., Mastepanov, M., Tamstorf, M. P., Eklundh, L., Schubert, P., Ekberg, A., Sigsgaard, C.,
1035 Christensen, T. R., and Ström, L.: High-resolution satellite data reveal an increase in peak growing
1036 season gross primary production in a high-Arctic wet tundra ecosystem 1992-2008, *Int. J. Appl. Earth
1037 Obs. Geoinf.*, 18, 407-416, 2012.

1038 Tagesson, T., Fensholt, R., Cropley, F., Guiro, I., Horion, S., Ehammer, A., and Ardö, J.: Dynamics in
1039 carbon exchange fluxes for a grazed semi-arid savanna ecosystem in West Africa, *Agr. Ecosyst.*
1040 *Environ.*, 205, 15-24, <http://dx.doi.org/10.1016/j.agee.2015.02.017>, 2015a.
1041 Tagesson, T., Fensholt, R., Guiro, I., Rasmussen, M. O., Huber, S., Mbow, C., Garcia, M., Horion, S.,
1042 Sandholt, I., Rasmussen, B. H., Göttsche, F. M., Ridler, M.-E., Olén, N., Olsen, J. L., Ehammer, A.,
1043 Madsen, M., Olesen, F. S., and Ardö, J.: Ecosystem properties of semi-arid savanna grassland in West
1044 Africa and its relationship to environmental variability, *Global Change Biol.*, 21, 250-264, doi:
1045 10.1111/gcb.12734, 2015b.
1046 Thenkabail, P. S., Smith, R. B., and De Pauw, E.: Hyperspectral Vegetation Indices and Their
1047 Relationships with Agricultural Crop Characteristics, *Remote Sens. Environ.*, 71, 158-182,
1048 [http://dx.doi.org/10.1016/S0034-4257\(99\)00067-X](http://dx.doi.org/10.1016/S0034-4257(99)00067-X), 2000.
1049 Thenkabail, P. S., Enclona, E. A., Ashton, M. S., and Van Der Meer, B.: Accuracy assessments of
1050 hyperspectral waveband performance for vegetation analysis applications, *Remote Sens. Environ.*, 91,
1051 354–376, 2004.
1052 Thenkabail, P. S., Lyon, J. G., and Huete, A.: Advances in hyperspectral remote sensing of vegetation
1053 and agricultural croplands, in: *Hyperspectral Remote Sensing of Vegetation*, edited by: Thenkabail, P.
1054 S., Lyon, J. G., and Huete, A., CRC Press, Taylor and Francis Group, Boca Raton, FL, 3-35, 2012.
1055 Tucker, C. J.: Red and photographic infrared linear combinations for monitoring vegetation, *Remote*
1056 *Sens. Environ.*, 8, 127-150, [http://dx.doi.org/10.1016/0034-4257\(79\)90013-0](http://dx.doi.org/10.1016/0034-4257(79)90013-0), 1979.
1057 van Leeuwen, W. J. D., Huete, A. R., and Laing, T. W.: MODIS Vegetation Index Compositing Approach:
1058 A Prototype with AVHRR Data, *Remote Sens. Environ.*, 69, 264-280, [http://dx.doi.org/10.1016/S0034-](http://dx.doi.org/10.1016/S0034-4257(99)00022-X)
1059 [4257\(99\)00022-X](http://dx.doi.org/10.1016/S0034-4257(99)00022-X), 1999.
1060 Verhoef, W., and Bach, H.: Coupled soil–leaf–canopy and atmosphere radiative transfer modeling to
1061 simulate hyperspectral multi-angular surface reflectance and TOA radiance data, *Remote Sens.*
1062 *Environ.*, 109, 166-182, <http://dx.doi.org/10.1016/j.rse.2006.12.013>, 2007.
1063 Vickers, D., and Mahrt, L.: Quality control and flux sampling problems for tower and aircraft data, *J.*
1064 *Atmos. Ocean. Tech.*, 14, 152-526, 1997.
1065 Webb, E. K., Pearman, G. I., and Leuning, R.: Correction of the flux measurements for density effects
1066 due to heat and water vapour transfer, *Q. J. Roy. Meteor. Soc.*, 106, 85-100, 1980.
1067 Wilczak, J. M., Oncley, S. P., and Stage, S. A.: Sonic anemometer tilt correction algorithms, *Bound.-Lay.*
1068 *Meteorol.*, 99, 127-150, 2001.

1069

1070

1071 **Tables**

1072 | Table 1. Information about the [sensor-instrumental](#) set-up for the measured environmental variables. HCRF is hemispherical conical reflectance
 1073 | factor; GPP is gross primary productivity; LUE is light use efficiency; and FAPAR is fraction of photosynthetically active radiation absorbed by the
 1074 | vegetation. Min and Max are minimum and maximum values measured, respectively; DW is dry weight; C is carbon; and MJ is mega joule. [The](#)
 1075 | [year started is the first year with measurements. Time is in UTC. For more information about the instrumental set-up, see](#) Tagesson et al.
 1076 | (2015b).

Variable	Year started	Unit	Sensors	Sensor company	Data size	Aggregation method	Data gaps	Min	Max
Hyperspectral HCRF	2011	-	Fieldspec 3	ASD Inc., Colorado, USA	371	Daily median	31%	0	1
Herbaceous biomass	2006	g DW m ⁻²	-	-	12	Daily mean 28 plots	-	0	223
GPP	2010	g C d ⁻¹	LI-7500, GILL R3	LI-COR Inc., Lincoln, USA; Gill instruments, Hampshire, UK	285	Daily sums	56%	- 14.22	- 0.22
LUE	2010	g C MJ ⁻¹	LI-7500, GILL R3	LI-COR Inc., Lincoln, USA; Gill instruments, Hampshire, UK	272	Daily estimates	28%	0.02	1.89
FAPAR	2004	-	Quantum SKP 215	Skye instruments Ltd., Llandridod wells, UK	369	Daily averages 10:00-16:00	1%	0.07	0.77

1077

1078

Table 2. Wavelengths of the hemispherical conical reflectance factors (HCRF) ($\rho_i, j; \text{nm}$) used in the normalized difference spectral indices (NDSI) that generated the strongest correlations with ecosystem properties. DW is dry weight; FAPAR is the fraction of ~~photosynthetically~~ photosynthetically active radiation absorbed by the vegetation; AVG is average; SD is standard deviation; RMSE is root-mean-square-error; and RRMSE is relative RMSE.

Ecosystem property	Sample size	ρ_i	ρ_j	R^2	Observation (AVG \pm SD)	RMSE	<u>RRMSE (%)</u>
Biomass (g DW m ⁻²)	12	587	705	0.88 \pm 0.07	153 \pm 59	28.4 \pm 8.7	<u>18.6\pm5.7</u>
Gross primary productivity (g C m ⁻² d ⁻¹)	285	518	556	0.86 \pm 0.02	-4.3 \pm 4.0	1.5 \pm 0.1	<u>34.9\pm2.3</u>
Light use efficiency (g C MJ ⁻¹)	272	688	436	0.81 \pm 0.02	0.53 \pm 0.65	0.26 \pm 0.02	<u>52.8\pm3.8</u>
FAPAR	369	399	1295	0.81 \pm 0.02	0.41 \pm 0.16	0.06 \pm 0.003	<u>14.6\pm0.7</u>

Figures

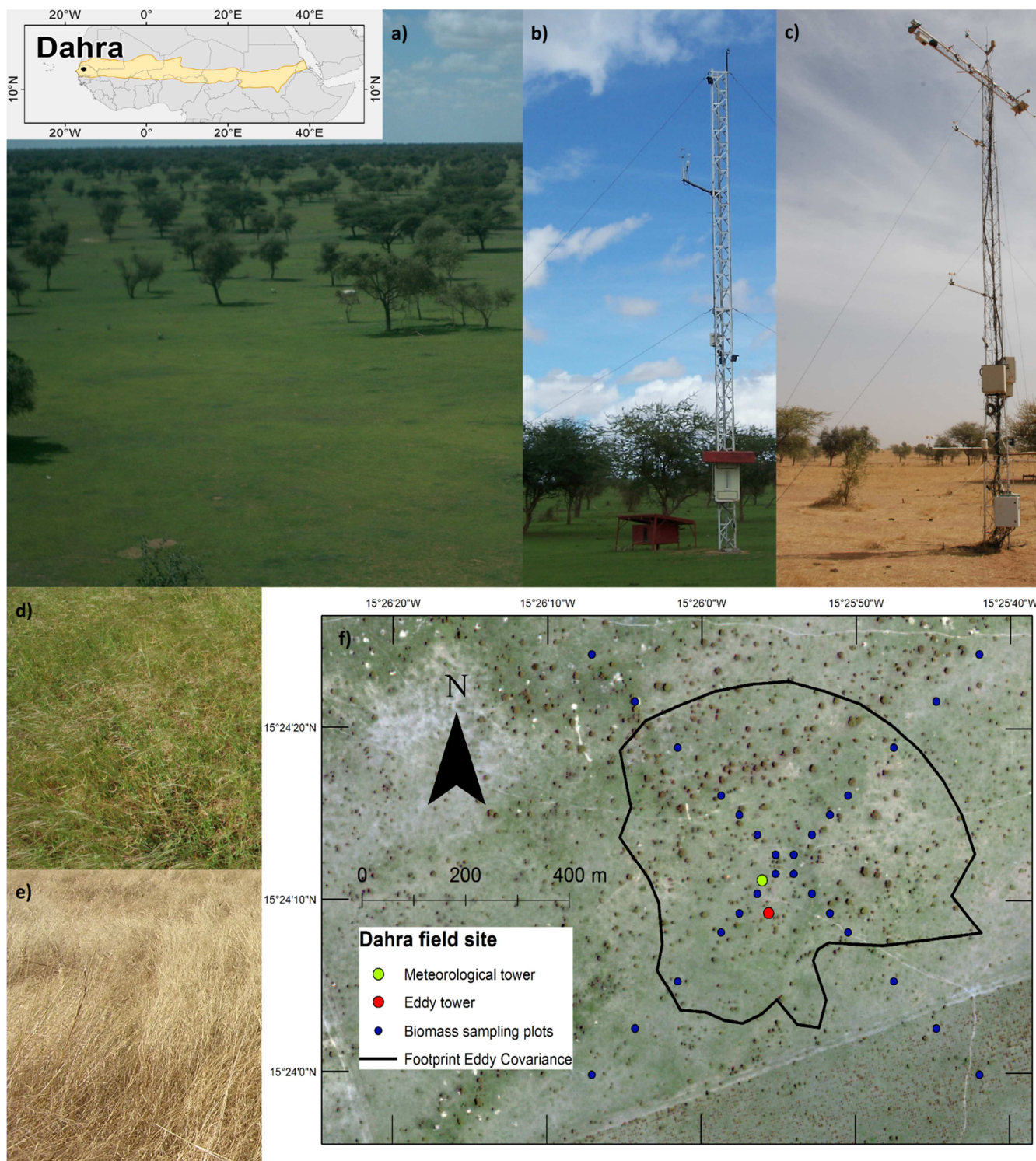
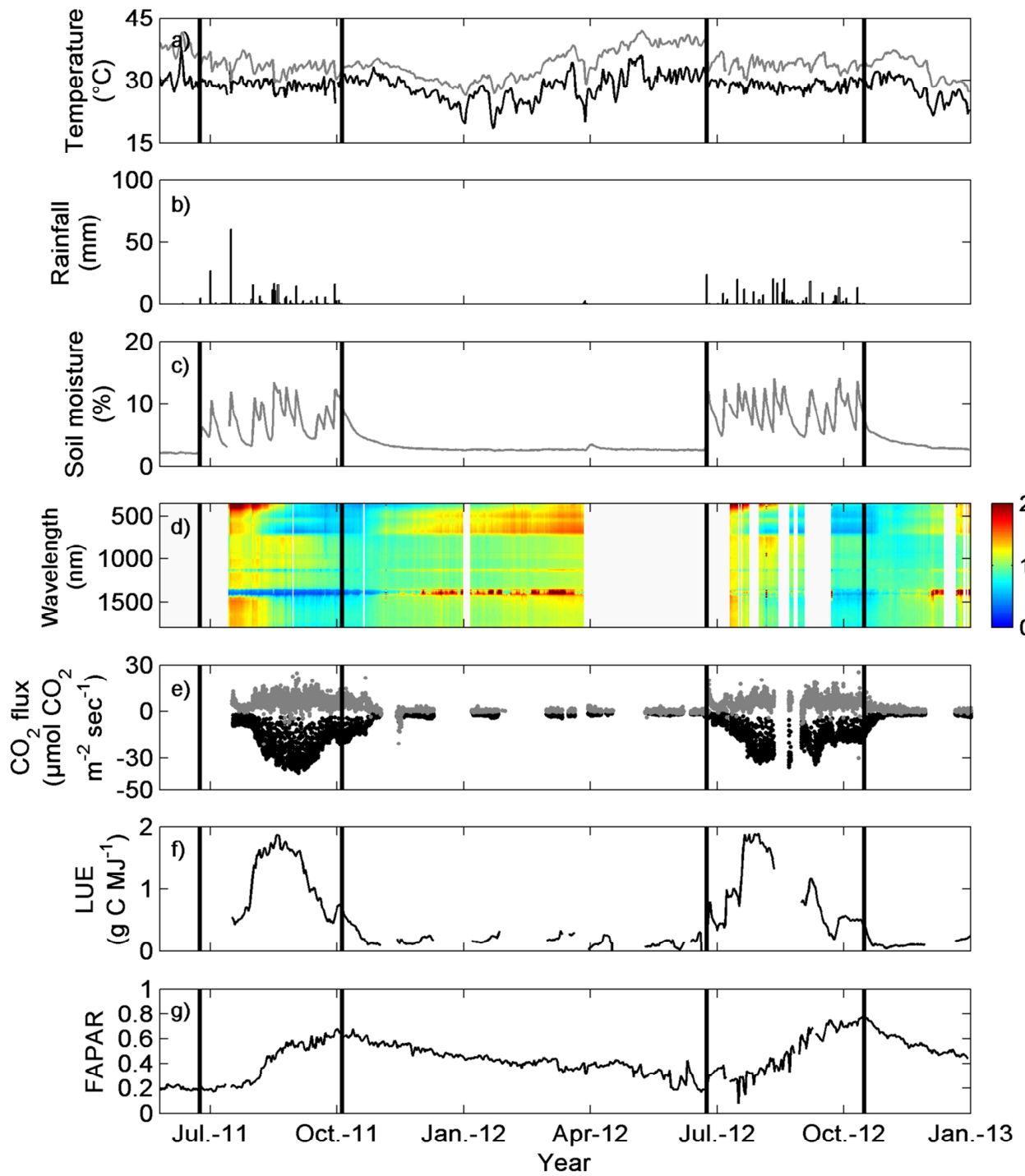


Figure 1. Map and photos of the Dahra field site and measured areas. The map shows the location of Dahra within the Sahel (orange area). a) Photo of the footprint of the eddy covariance (EC) tower; b) photo of the EC tower; c) photo of the meteorological tower with the spectroradiometers; d) photo of the instantaneous field of view (IFOV) of the spectroradiometers during the rainy season; e) photo of the IFOV of the

spectroradiometer during the beginning of the dry season; and f) Quickbird image from the Dahra field site from 11 September 2011 showing the location of the meteorological tower, the EC tower, the biomass sampling plots and the footprint of the EC measurements. The EC footprint area is the median 70% ~~cummulative~~cumulative flux distance from the eddy covariance tower. The photos of the EC tower and its footprint are taken during the rainy season whereas the photo of the meteorological tower shows the late dry season.



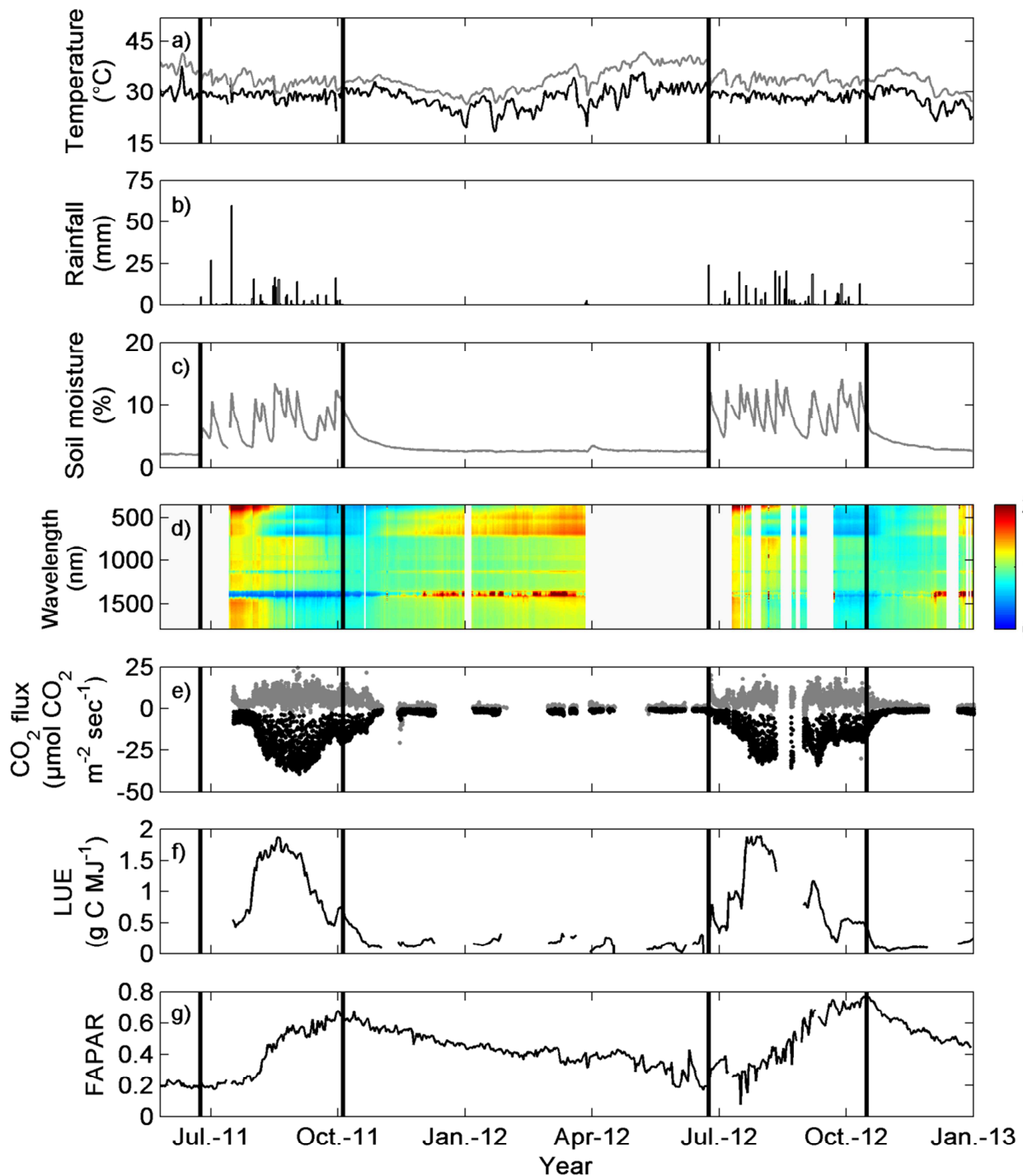
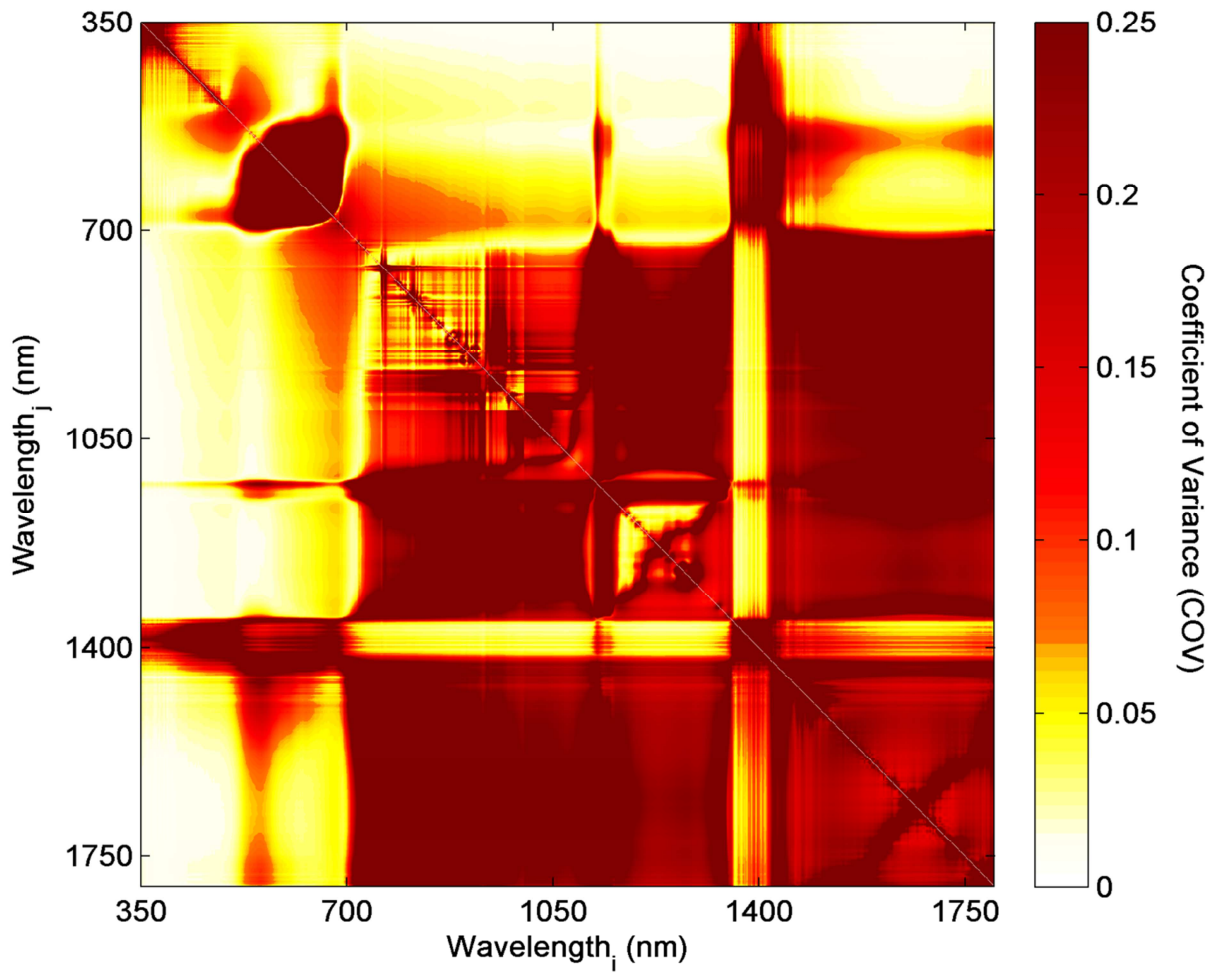


Figure 2. Time series of the measured variables: a) daily averaged air temperature (black line), and soil temperature at 0.05 m depth (grey line), b) daily sums of rainfall, c) daily average of soil moisture at 0.05 m depth, d) hyperspectral hemispherical conical reflectance factor (HCRF) normalized by calculating the ratio between daily median HCRF for each wavelength (350-1800 nm) and the average HCRF for the entire measurement period, e) gross primary productivity (GPP) (black dots) and ecosystem respiration (grey dots), f) the light use efficiency (LUE), and g) the fraction of photosynthetically active radiation absorbed by the vegetation (FAPAR). The black

vertical lines are the start and end of the rainy seasons (first and final day of rainfall). The gaps are caused by technical issues due to loss of power supply, broken sensors or filtering of data due to bad weather conditions.



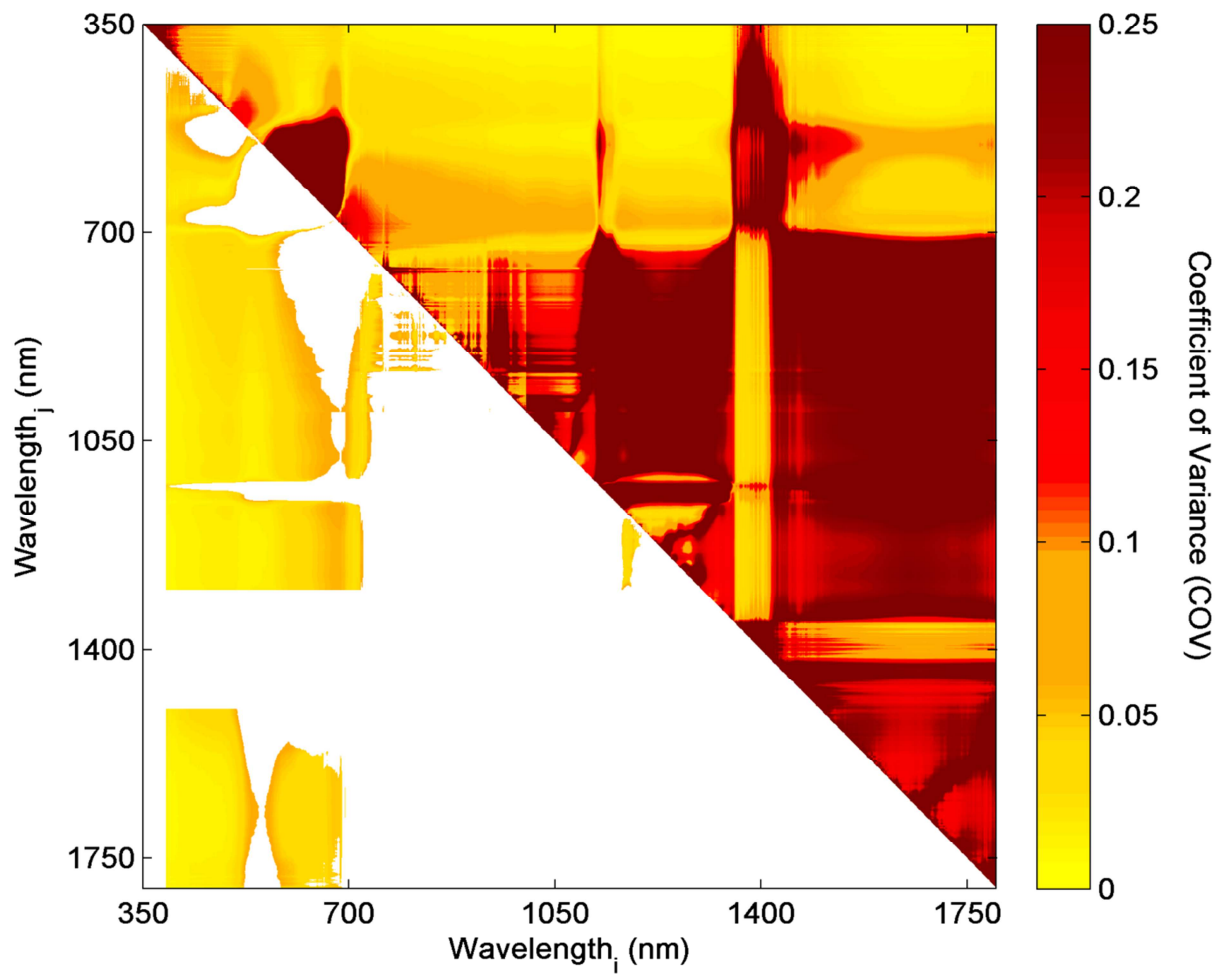
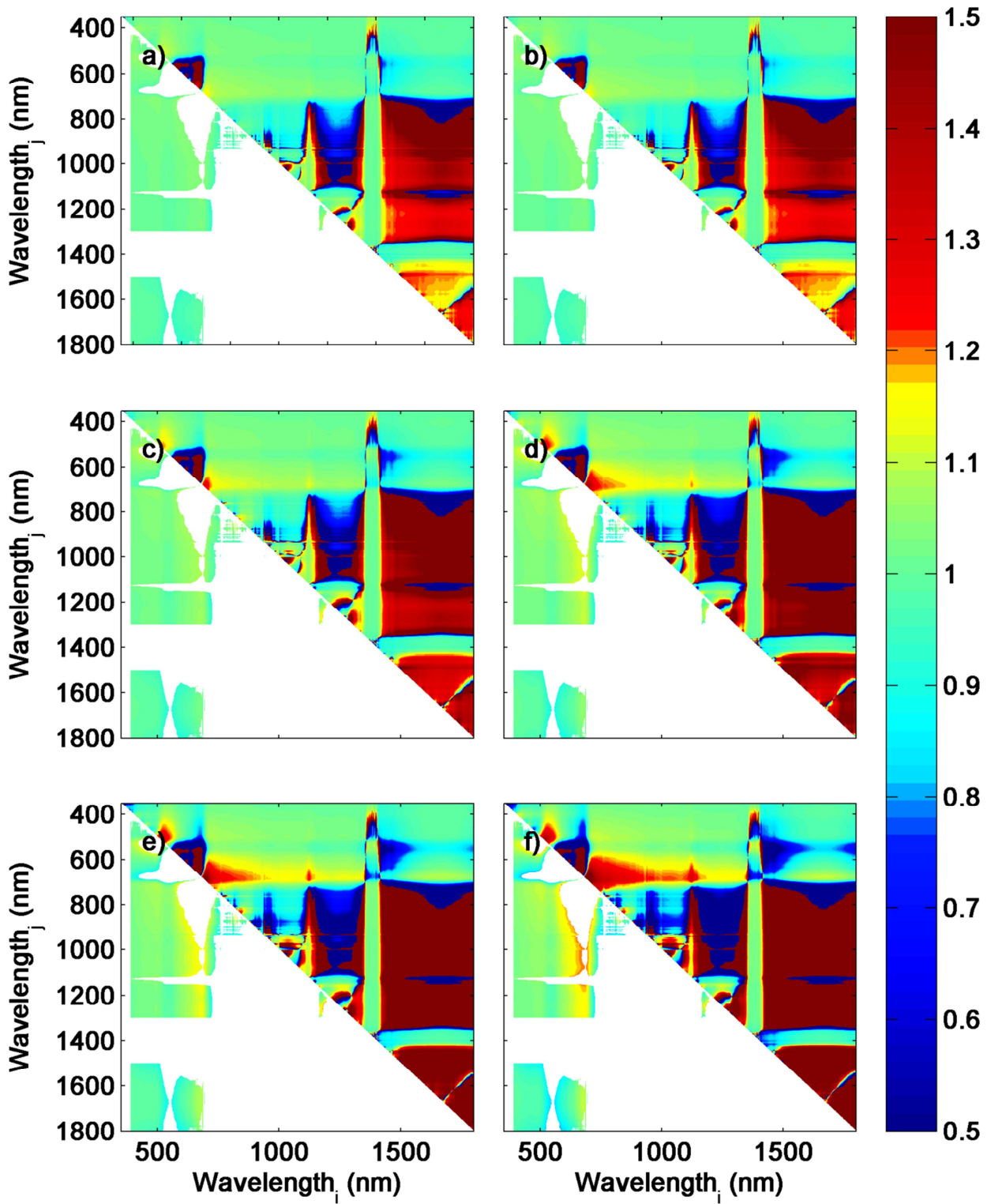


Figure 3. The coefficient of variation (COV), i.e. the ratio between daily standard deviation and the daily mean (measurements taken between 8:00 and 18:00 (UTC)), for different normalised difference spectral index (NDSI) wavelength (i, j) combinations for 12 days at the peak of the growing season 2011 (day of year 237-251; $n=576$). The COV indicates how strongly the NDSI are affected by variable sun angles. The upper right half of the chart shows the unfiltered R^2 values, whereas the lower left half shows filtered R^2 , based on the filtering criteria described under Subsect. 2.6.



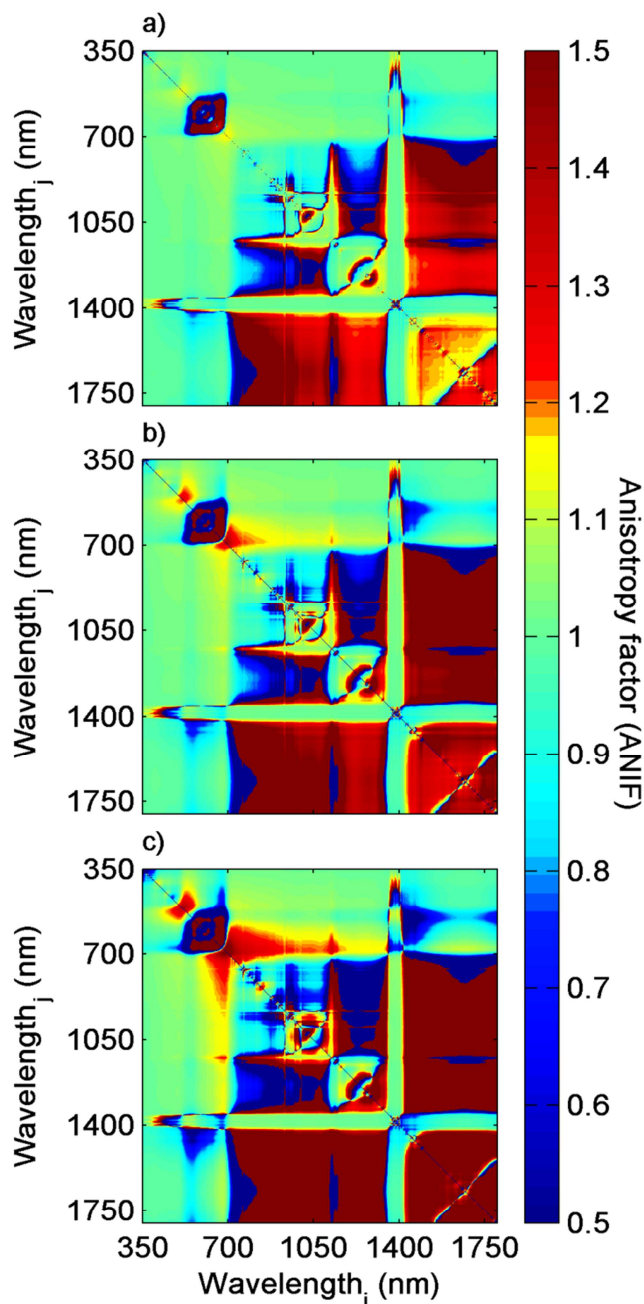


Figure 4. The anisotropy factor (ANIF) for different normalised difference spectral index (NDSI) wavelength (i, j) combinations for 15 days at the peak of the growing season 2011 (day of year 237-251) for the different sensor viewing angles: a) 15°E , b) 15°W , c) 30°E , d) 30°W , e) 45°E , and f) 45°W . The sensor is pointing east and west in the lower left and upper right corners of each plot, respectively. In order not to include effects of solar zenith angles in the analysis, only data measured between 12:00 and 14:00 (UTC) were used in the ANIF calculations ($n=48$). The upper right half of each chart shows the unfiltered R^2 values, whereas the lower left half shows filtered R^2 , based on the filtering criteria described under Subsect. 2.6.

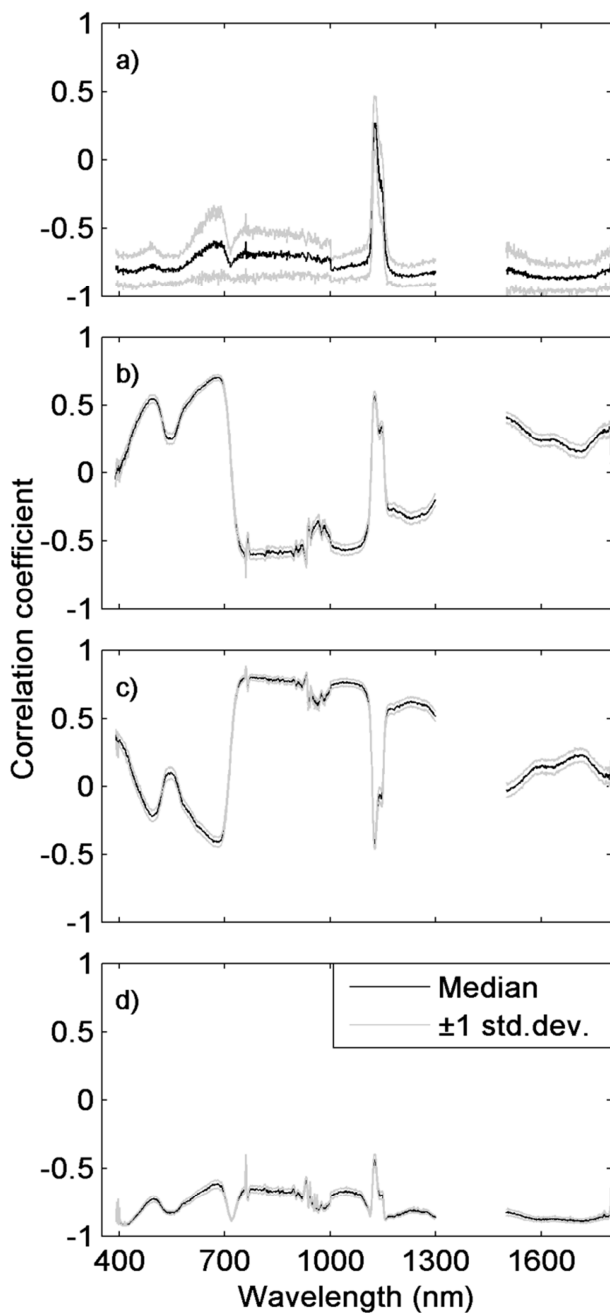
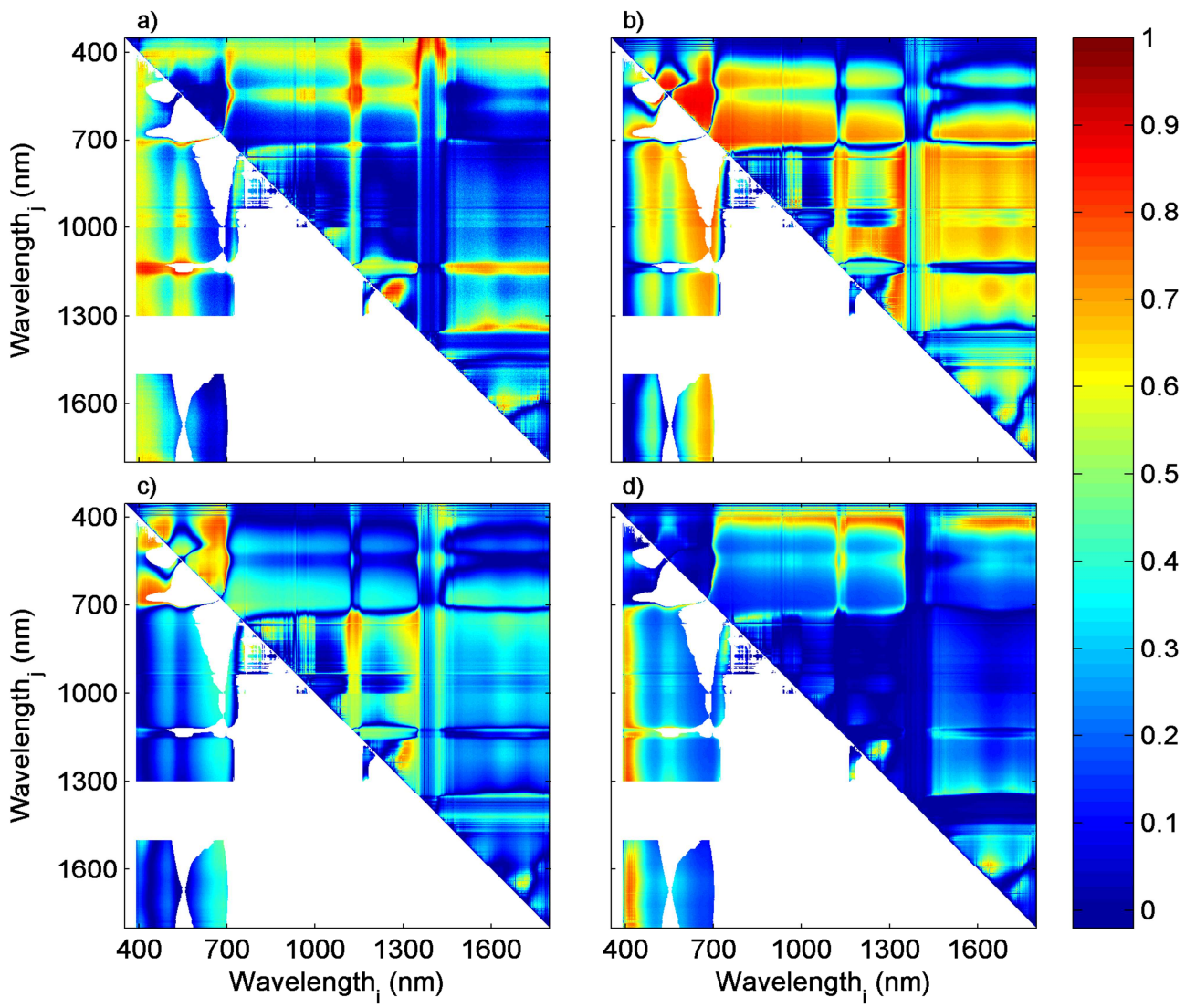


Figure 5. Median correlation coefficient (± 1 standard deviation) between seasonal dynamics in hyperspectral hemispherical conical reflectance factors (HCRF) 2011-2012 and a) dry weight biomass ($n=12$; g m^{-2}), b) gross primary productivity (GPP) ($n=285$; g C day^{-1}), c) light use efficiency (LUE) ($n=272$; g C MJ^{-1}), and d) fraction of photosynthetically active radiation absorbed by the vegetation (FAPAR) ($n=369$). The water absorption band (1300-1500 nm) was removed as it is strongly sensitive to atmospheric water content, and wavelengths between 350 and 390 nm were removed owing to low signal to noise ratio in the ASD sensors.



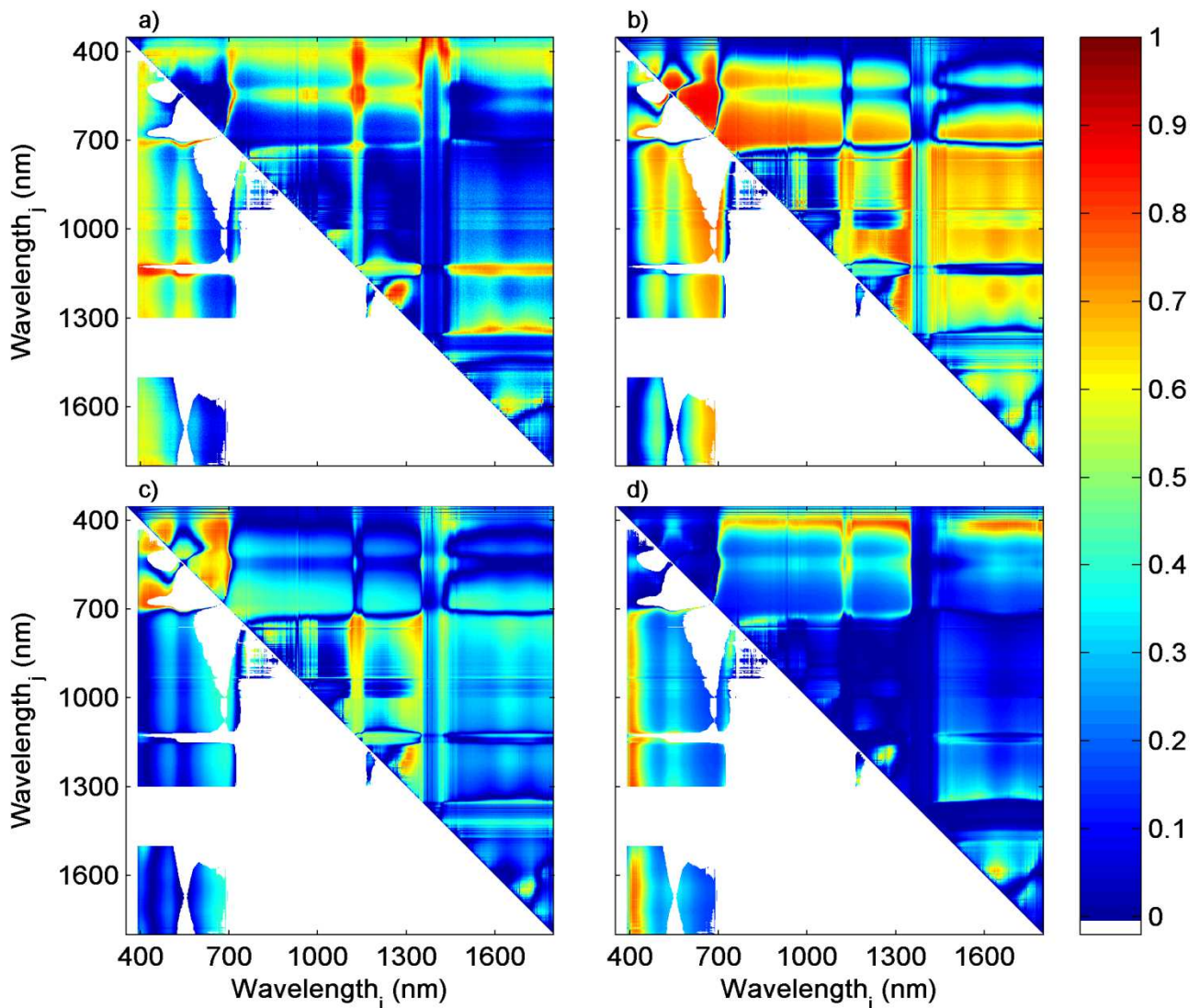


Figure 6. Coefficient of determination (R^2) between normalised difference spectral index (NDSI) and a) dry weight biomass ($n=12$; g m^{-2}), b) gross primary productivity (GPP) ($n=285$; g C day^{-1}), c) light use efficiency (LUE) ($n=272$; g C MJ^{-1}), and d) fraction of photosynthetically active radiation absorbed by the vegetation (FAPAR) ($n=369$). The upper right half of each [image-chart](#) shows the unfiltered R^2 values, whereas the lower left half shows filtered R^2 , based on the filtering criteria described under Subsect. 2.6.

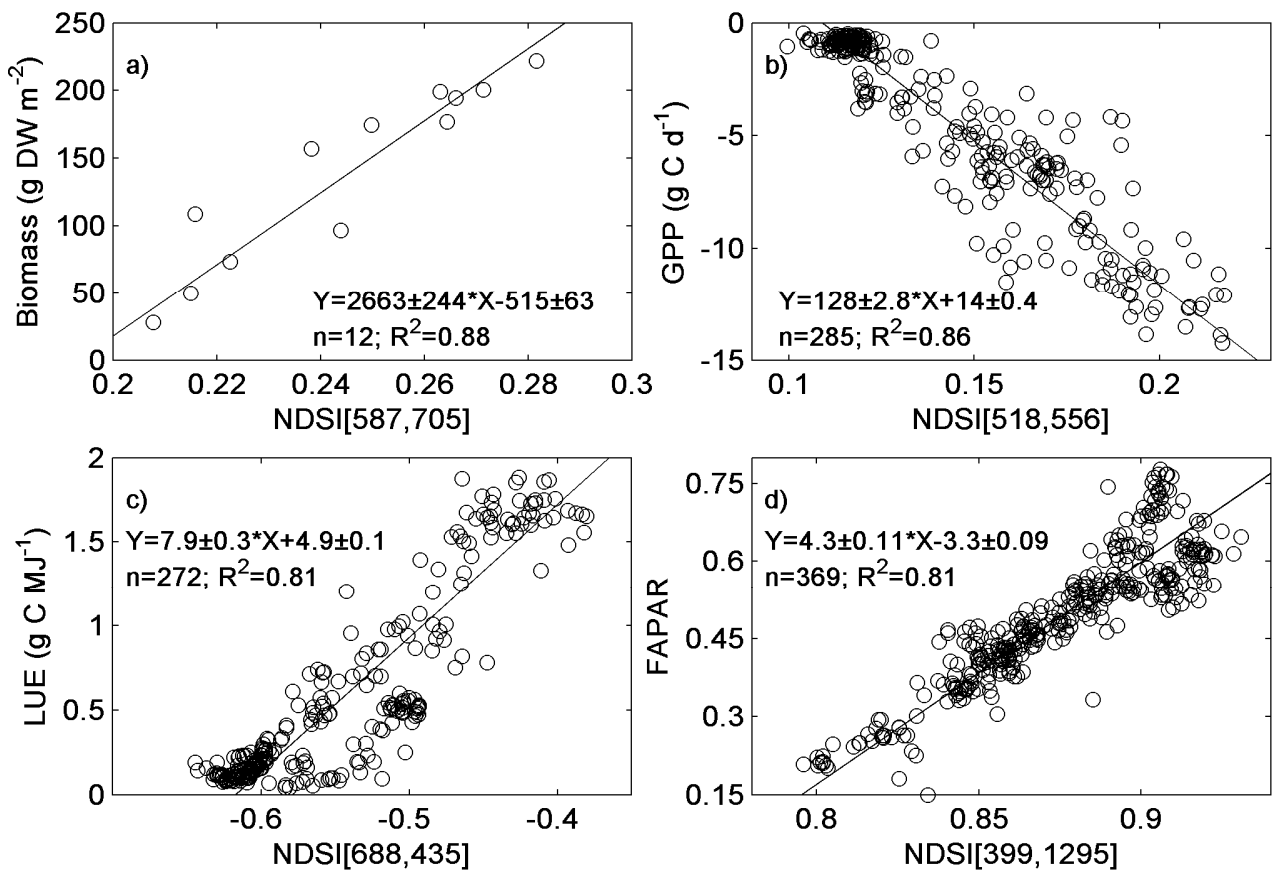


Figure 7. The least square linear regressions with the strongest relationships between the normalised difference spectral index (NDSI) and a) dry weight biomass, b) gross primary productivity (GPP), c) light use efficiency (LUE), and d) fraction of photosynthetically active radiation absorbed by the vegetation (FAPAR). In the equations, the slope and intercepts (\pm standard deviation) is given.